(12)

AD-F300008

ADA 112263

AD

TECHNICAL REPORT ARBRL-TR-02387

NUMERICAL EXPERIMENTS ON THE SHOCK SENSITIVITY OF MUNITIONS

Y. K. Huang
A. L. Arbuckle

January 1982

US ARMY ARMAMENT RESEARCH AND DEVELOPMENT COMMAND
BALLISTIC RESEARCH LABORATORY
ABERDEEN PROVING GROUND, MARYLAND

UNCLASSIFIED

SECURITY CLASSIFICATION OF THIS PAGE (When Data Entered)

REPORT DOCUMENTATION PAGE

READ INSTRUCTIONS BEFORE COMPLETING FORM

1. REPORT NUMBER: Technical Report ARBRL-TR-02387	2. GOVT ACCESSION NO.: AD-A112 263
3. RECIPIENT'S CATALOG NUMBER	
4. TITLE (and Subtitle): NUMERICAL EXPERIMENTS ON THE SHOCK SENSITIVITY OF MUNITIONS	5. TYPE OF REPORT & PERIOD COVERED: Final
	6. PERFORMING ORG. REPORT NUMBER
7. AUTHOR(s): Y. K. Huang and A. L. Arbuckle	8. CONTRACT OR GRANT NUMBER(s)
9. PERFORMING ORGANIZATION NAME AND ADDRESS: US Army Ballistic Research Laboratory (ATTN: DRDAR-BLT) Aberdeen Proving Ground, MD 21005	10. PROGRAM ELEMENT, PROJECT, TASK AREA & WORK UNIT NUMBERS: 1L162603AH18
11. CONTROLLING OFFICE NAME AND ADDRESS: US Army Armament Research and Development Command US Army Ballistic Research Laboratory (ATTN: DRDAR-BL) Aberdeen Proving Ground, MD 21005	12. REPORT DATE: JANUARY 1982
	13. NUMBER OF PAGES: 56
14. MONITORING AGENCY NAME & ADDRESS(if different from Controlling Office)	15. SECURITY CLASS. (of this report): UNCLASSIFIED
	15a. DECLASSIFICATION/DOWNGRADING SCHEDULE

16. DISTRIBUTION STATEMENT (of this Report)

Approved for public release; distribution unlimited.

17. DISTRIBUTION STATEMENT (of the abstract entered in Block 20, if different from Report)

18. SUPPLEMENTARY NOTES

19. KEY WORDS (Continue on reverse side if necessary and identify by block number)

C-J (Chapman-Jouguet)	Munitions Vulnerability	Pop Plot
Detonation	Numerical Simulation	Reactive Hydrodynamics
Explosives	Parameter Analysis	Shock Hugoniot/Waves
Forest Fire Model	Plastic Shields	Shock Initiation/Sensitivity

20. ABSTRACT (Continue on reverse side if necessary and identify by block number) (dlc)

This work is concerned with shock initiation in munitions. As a numerical experiment, twenty computations have been performed to simulate three basic types of detonation transfer between munitions at small separations. All computations show two distinct reactive flows, with shock waves communicable between them. The numerical aspects of these can serve to explain the mechanism and development of the detonation phenomena. One after the other, shock pulses arrive at the munition or acceptor explosive; it is the impact shock pulse,

(continued)

DD FORM 1 JAN 73 1473 EDITION OF 1 NOV 65 IS OBSOLETE

UNCLASSIFIED

SECURITY CLASSIFICATION OF THIS PAGE (When Data Entered)

20. Abstract (continued)

whose peak rises above the large scale gap test 50% point, that builds up to detonation. Shock sensitivity of the munition decreases as casing thickness or interround separation increases. Our numerical experiments also demonstrate the remarkable efficacy of thin plastic shields in suppressing detonation transfer.

TABLE OF CONTENTS

Page

LIST OF ILLUSTRATIONS 5

LIST OF TABLES 7

I. INTRODUCTION 9

A. Background 9

B. Statement of Problem 10

II. NUMERICAL APPROACH 14

A. Reactive Hydrodynamic Code 2DE 14

B. Application to NOL Gap Test 16

C. Application to Munitions Problem 16

III. RESULTS AND DISCUSSION 20

A. Flow and Shock Patterns of Interactive Munitions 20

1. Reactive Flows within Donor and Acceptor 20

2. Propagation of Reactive and Inert Shock Waves 20

3. Description by Contour Plots 27

B. Response of Reactive Acceptors 32

1. Shock Initiation 32

2. Effects of Parameter Variations 32

C. Response of Inert Acceptors 45

1. Shock Loading 45

2. Effects of Parameter Variations 46

D. Effects of Plastic Shield between Rounds 47

IV. SUMMARY AND CONCLUSION 52

ACKNOWLEDGEMENTS 54

DISTRIBUTION LIST 55

LIST OF ILLUSTRATIONS

Figure		Page
1	Configuration of Interround Propagation Experiment	11
2	Schematic of Configuration for Numerical Simulation	12
3	Computational Sketch of NOL Gap Test	17
4	Density Contours for NOL Gap Test	18
5	Mass Fraction Contours for NOL Gap Test	19
6	Shock Pressure versus Distance and Time for Two Rounds in Contact (Reactive, $R/R_o = 1.0$)	21
7	Shock Pressure versus Distance and Time for Two Rounds in Contact (Inert, $R/R_o = 1.0$)	22
8	Shock Pressure versus Distance and Time for Two Rounds Separated (Reactive, $R/R_o = 1.5$)	23
9	Shock Pressure versus Distance and Time for Two Rounds Separated (Inert, $R/R_o = 1.5$)	24
10	Shock Pressure versus Distance and Time for Two Rounds Separated (Reactive, $R/R_o = 2.0$)	25
11	Shock Pressure versus Distance and Time for Two Separated Rounds (Inert, $R/R_o = 2.0$)	26
12	Converging Shock Profiles in Donors with Various Separation and Casing Thickness	28
13	Converging Shock Formed in Inert Acceptor with $R/R_o = 1.0$ and $r/R_o = 0.27$	29
14	Isobars of Two Rounds in Contact (Reactive, $R/R_o = 1.0$)	30
15	Mass-Fraction Contours of Two Rounds in Contact (Reactive, $R/R_o = 1.0$)	31
16	Sketch Showing Deformation of Two Rounds in Contact (Reactive, $R/R_o = 1.0$, $r/R_o = 0.15$)	33
17	Schematic of Shock Trajectory for Heterogeneous Initiation Process	34
18	Effects of Interround Separation on Time to Reaction	37
19	Effects of Casing Thickness on Time to Reaction	38

LIST OF ILLUSTRATIONS (continued)

Figur		Page
20	Effects of Interround Separation on Time to Detonation	39
21	Effects of Casing Thickness on Time to Detonation.	40
22	Effects of Interround Separation on Initial Shock Pressure	41
23	Effects of Casing Thickness on Initial Shock Pressure.	42
24	Effects of Interround Separation on Average Velocity of Shock Buildup.	43
25	Effects of Casing Thickness on Average Velocity of Shock Buildup.	44
26	Effects of Interround Separation on Inert Shock Loading.	48
27	Effects of Casing Thickness on Inert Shock Loading	49
28	Inert Response Measured with P^2t Criterion	50
29	N-Shape Curve Showing Variation of Time to Reaction with Shield Thickness	53

LIST OF TABLES

TABLE		Page
I.	Rounds in Contact	10
II.	Rounds Separated by Air Gap	13
III.	Rounds Separated by Plastic Shield	13
IV.	Shock Initiation Results	35
V.	Shock Loading Results	46
VI.	Results of Shock Initiation with Plastic Shield	51

I. INTRODUCTION

A. Background

In an armory or a depot, in transport on land or sea, and while carried in combat vehicles, munitions are packed into magazines, pallets, or milvans. Such logistic stores must be protected against the risk of mass detonation. Various modes of interround communication of violent reaction have been investigated by Howe and co-workers[1-6]. One of their objectives was to find predictive criteria which could be used to reduce the vulnerability of munitions in hazardous environments.

Generally, munitions are sensitive to stimuli[1] such as explosive shock, air blast, fragment impact, and fire. An accidental explosion of a single round could spread throughout the entire store. This is referred to as munitions fratricide and mass detonation[1,3]. Since it would be too difficult to assess all processes involved in such an event, we consider in this work the shock-induced phenomena only. We have chosen to do so for two additional reasons. First, shock initiation processes dominate the early stages of an interround propagation problem especially when the separation is small. Second, these processes are amenable to numerical analysis which incorporates material constants and data in reactive hydrodynamic codes. We have used the 2DE code[7,8] to carry out this investigation via a series of computations. As experimental data are scarce, this investigation is of an exploratory nature. It should be noted that our calculated results furnish

---

[1] *Howe, P. M., "The Phenomenology of Interround Communication and Techniques for Prevention," Ballistic Research Laboratory Technical Report ARBRL-TR-02048 (March 1978).* ADA 054373

[2] *Howe, P. M., "The Response of Munitions to Impact," Ballistic Research Laboratory Technical Report ARBRL-TR-02169 (June 1979).* ADB 040230L

[3] *Howe, P. M., "An Approach to the Development of Hardened Munitions, Part A-Warheads," Ballistic Research Laboratory Special Publication ARBRL-SP-00010 (June 1979).* ADB 038925L

[4] *Frey, R., Howe, P. M., Trimble, J., and Melani, G., "Initiation of Explosive Charges by Projectile Impact," Ballistic Research Laboratory Technical Report ARBRL-TR-02176 (June 1979).* ADB 041931L

[5] *Howe, P. M. and Collis, D., "Effectiveness of Plastic Shields in Prevention of Propagation of Reaction between Compartmentalized Warheads," Ballistic Research Laboratory Memorandum Report ARBRL-MR-02827 (April 1978).* ADB 027466L

[6] *Howe, P. M. and Jackson, W., "An Experimental Study of the Cookoff Hazard of Compartmentalized Tank Projectiles," Ballistic Research Laboratory Memorandum Report ARBRL-MR-2666 (August 1976).* ADB 014010L

[7] *Mader, C. L., "Numerical Modeling of Detonations," (University of California Press, 1979).*

[8] *Kershner, J. D. and Mader, C. L., "2DE: A Two Dimensional Continuous Eulerian Hydrodynamic Code for Computing Multicomponent Reactive Hydrodynamic Problems," Los Alamos Scientific Laboratory Technical Report LA-4846, (March 1972).*

considerable details which are not readily obtainable using other approaches. These results also disclose certain trends which may be used for predictive purposes.

In what follows, we shall formulate the munitions sensitivity problem with input data adequate to facilitate its numerical solution.

B. Statement of Problem

Let us consider the detonation transfer between two adjacent munition rounds as shown in Figure 1 (corresponding to an experimental configuration of Reference 1). In a gap-test analogy, we may refer to one round as the donor and the other as the acceptor. Of course, the explosives in both the donor and acceptor are essential for the detonation transfer here. Casings, ambient air, and any plastic shield form the "gap" or shock attenuator. For computational purposes, we further idealize the interround layout to two dimensions as shown in Figure 2. The symbols R_o, R, r, and h are defined in Figure 2, and we use the parameters R/R_o, r/R_o, and h/R_o to characterize our computational problem. We shall only consider interround separations within the range $1 \leq R/R_o \leq 2$, since this is the region in which shock initiation is expected to dominate. Note that the lower limit ($R/R_o = 1$) represents the mode of propagation of the gap test. Above the upper limit, fragment impact dominates the initiation process. Between these two extremes, shocks caused by casing impact contribute to the processes of interround communication, and we have used $R/R_o = 1.5$ as a typical value for sample calculations. In another group of computations with $R/R_o = 1.5$, plastic shields of various thicknesses, h/R_o, are included in the middle of the air gap. We have considered three basic types of interround problem as summarized in Tables I through III. These consist of twenty cases all with $R_o = 52.5$ mm and composition-B as the donor charge initiated on its axis.

The five cases of Table I refer to two rounds in contact ($R/R_o = 1.0$, $h/R_o = 0$). Columns 4-9 describe the computational specifications for the

TABLE I

ROUNDS IN CONTACT

Case	r/R_o	Acceptor	$\Delta X, \Delta Y$ (mm)	I	J	IJ (cells)	Δt (μsec)	N (cycles)
A-1	0.15	PBX-9205	1.944	50	135	6,750	0.05	600
A-2	0.20	PBX-9205	1.944	50	135	6,750	0.05	600
A-3	0.27	PBX-9205	1.944	50	135	6,750	0.05	600
A-1n	0.15	Inert PBX-9205	1.944	50	135	6,750	0.05	700
A-3n	0.27	Inert PBX-9205	1.981	50	130	6,500	0.05	900

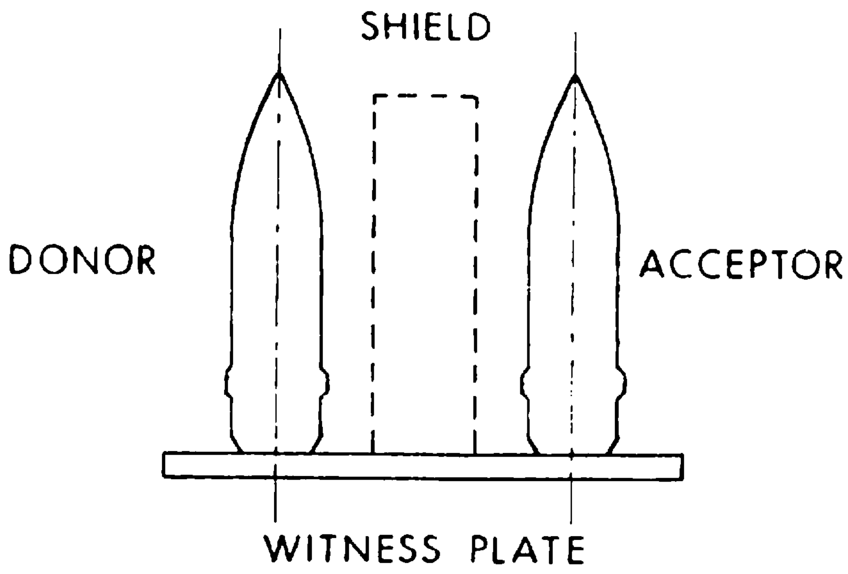

Figure 1 - Configuration of Interround Propagation Experiment

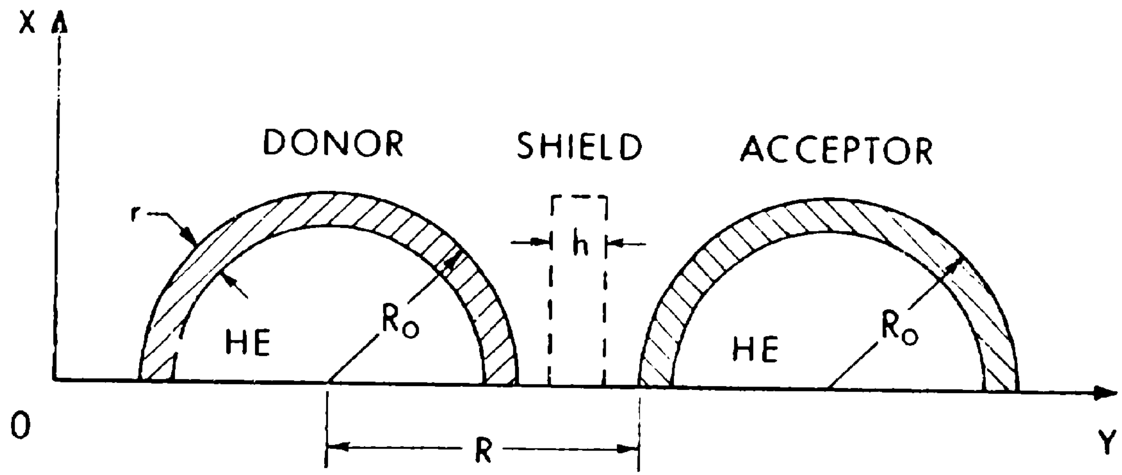

Figure 2 - Schematic of Configuration for Numerical Simulation

2DE code, which will be explained later. The nonreactive computations A-1n and A-3n were performed to examine shock loading, with all input data the same as in A-1 and A-3 respectively.

The ten computations of Table II describe the second type of sensitivity problem, i.e., two rounds separated by an air gap (R/R_o = 1.5 and 2.0, h/R_o = 0).

TABLE II

ROUNDS SEPARATED BY AIR GAP

Case	r/R_o	R/R_o	Acceptor	$\Delta X, \Delta Y$ (mm)	I	J	IJ (cells)	Δt (μsec)	N (cycles)
B-1	0.15	1.5	PBX-9205	1.981	50	150	7,500	0.05	900
B-2	0.20	1.5	PBX-9205	1.944	50	150	7,500	0.05	900
B-3	0.27	1.5	PBX-9205	1.981	50	150	7,500	0.05	900
C-1	0.15	2.0	PBX-9205	1.981	50	160	8,000	0.05	1,000
C-2	0.20	2.0	PBX-9205	1.944	50	165	8,250	0.05	1,000
C-3	0.27	2.0	PBX-9205	1.981	50	160	8,000	0.05	1,000
B-1n	0.15	1.5	Inert	1.981	50	145	7,250	0.05	900
B-3n	0.27	1.5	Inert	1.981	50	145	7,250	0.05	900
C-1n	0.15	2.0	Inert	1.981	50	155	7,750	0.05	900
C-3n	0.27	2.0	Inert	1.981	50	155	7,750	0.05	900

Five cases with plastic shields and R/R_o = 1.5 are listed in Table III. These are similar to the B's of Table II except that a plastic shield is inserted at the midpoint of the air gap.

TABLE III

ROUNDS SEPARATED BY PLASTIC SHIELD

Case	r/R_o	h/R_o	Acceptor	$\Delta X, \Delta Y$ (mm)	I	J	IJ (cells)	Δt (μsec)	N (cycles)
D-1	0.20	0.20	PBX-9205	1.810	50	150	7,500	0.04	800
D-2	0.20	0.28	PBX-9205	1.810	50	150	7,500	0.04	800
D-3	0.20	0.38	PBX-9205	1.810	50	150	7,500	0.04	800
D-4	0.20	0.47	PBX-9205	1.810	50	150	7,500	0.04	900
D-5	0.15	0.14	PBX-9205	1.810	50	150	7,500	0.04	1,000

In all the computations summarized in Tables I through III, only five materials are involved: composition-B (64% RDX, 36% TNT), PBX-9205 (92% RDX, 6% polystyrene, 2% DOP), steel, air, and Plexiglas. In order to perform the computations, we used the equation-of-state and shock-initiation constants of Reference 9. Such a large number of material constants may appear rather inconvenient to someone who is not familiar with the computer code 2DE. It should be noted that the constants have been all calibrated with established data from reliable sources (e.g., handbooks, journal papers, laboratory reports). In fact, several subprograms of 2DE are executed one after the other, each calling for one or two dozen of such constants as input. Combined numerical results turn out to offer a close simulation of many detonation phenomena. From a computational point of view, it is not excessive to use the set of constants as mentioned.

II. NUMERICAL APPROACH

A. Reactive Hydrodynamic Code 2DE

The computer code adopted for this investigation is 2DE, a two-dimensional Eulerian hydrodynamic code developed at Los Alamos National Laboratory for reactive flow problems[7,8]. It is a large code with several features not available in other codes (e.g., HEMP, HELP). The following are the nine equations which are used in 2DE for describing the reactive flow of detonation phenomena:

$$\frac{\partial \rho}{\partial t} + U\frac{\partial \rho}{\partial R} + V\frac{\partial \rho}{\partial Z} = -\rho\left(\frac{\partial U}{\partial R} + \frac{\partial V}{\partial Z} + \frac{\alpha-1}{R}U\right) \tag{1}$$

$$\rho\left(\frac{\partial U}{\partial t} + U\frac{\partial U}{\partial R} + V\frac{\partial U}{\partial Z}\right) = \frac{\partial}{\partial R}\left(S_{RR} - P\right) + \frac{\partial S_{ZZ}}{\partial Z} + \frac{\alpha-1}{R}\left(2S_{RR} + S_{ZZ}\right) \tag{2}$$

$$\rho\left(\frac{\partial V}{\partial t} + U\frac{\partial V}{\partial R} + V\frac{\partial V}{\partial Z}\right) = \frac{\partial S_{RZ}}{\partial R} + \frac{\partial}{\partial Z}\left(S_{ZZ} - P\right) + \frac{\alpha-1}{R}S_{RZ} \tag{3}$$

$$\rho\left(\frac{\partial I}{\partial t} + U\frac{\partial I}{\partial R} + V\frac{\partial I}{\partial Z}\right) = -P\left(\frac{\partial U}{\partial R} + \frac{\partial V}{\partial Z} + \frac{\alpha-1}{R}U\right) + S_{RR}\left(\frac{\partial U}{\partial R} - \frac{\alpha-1}{R}U\right) + S_{ZZ}\left(\frac{\partial V}{\partial Z} - \frac{\alpha-1}{R}U\right) + S_{RZ}\left(\frac{\partial U}{\partial Z} + \frac{\partial V}{\partial R}\right) \tag{4}$$

$$P = p + q = p(\rho, I, W) + q\left(K\rho\frac{\partial U}{\partial R}, K\rho\frac{\partial V}{\partial Z}\right) \tag{5}$$

$$-\frac{1}{W}\left(\frac{\partial W}{\partial t} + U\frac{\partial W}{\partial R} + V\frac{\partial W}{\partial Z}\right) = \exp\left(C_o + C_1P + C_2P^2 + .. + C_nP^n\right) \tag{6}$$

$$\frac{\partial S_{RR}}{\partial t} = 2\mu\left(\frac{\partial U}{\partial R} + \frac{1}{3\rho}\frac{\partial \rho}{\partial t}\right) + S_{RZ}\left(\frac{\partial U}{\partial Z} - \frac{\partial V}{\partial R}\right) \tag{7}$$

$$\frac{\partial S_{ZZ}}{\partial t} = 2\mu\left(\frac{\partial V}{\partial Z} + \frac{1}{3\rho}\frac{\partial \rho}{\partial t}\right) - S_{RZ}\left(\frac{\partial U}{\partial Z} - \frac{\partial V}{\partial R}\right) \tag{8}$$

$$\frac{\partial S_{RZ}}{\partial t} = 2\mu\left(\frac{\partial U}{\partial Z} + \frac{\partial V}{\partial R}\right) - \frac{1}{2}\left(S_{RR} - S_{ZZ}\right)\left(\frac{\partial U}{\partial Z} - \frac{\partial V}{\partial R}\right) \tag{9}$$

---

[9] *Bowman, A. L., Kershner, J. D., and Mader, C. L., "A Numerical Model of the Gap Test," Los Alamos Scientific Laboratory Technical Report LA-8408, (October 1980).*

where ρ, U, V, W, P, I, S_{RR}, S_{ZZ} and S_{RZ} denote the density, radial velocity, axial velocity, mass fraction of unreacted explosive, pressure, internal energy, radial deviatoric stress, axial deviatoric stress, and shear stress respectively (R, Z, and t being the pertinent coordinates and time with $\alpha = 1$ for rectangular and 2 for cylindrical coordinates). The total pressure P is the sum of two parts: the thermodynamic pressure p and the artificial viscous stress q for the treatment of shock waves (with coefficient K = constant). Five subroutines are available[7,8] for the equation-of-state computation. These are called HOM, HOM2S, HOMSG, HOM2G, and HOM2SG. They are used for computing simple and mixed cells in pressure and/or temperature equilibrium (temperature T is calculated according to the Walsh-Christian scheme). The reaction rate associated with heterogeneous shock initiation of an explosive is given by Equation (6) with n = 14 or 15 (i.e., Forest Fire burn[7] using fourteen or fifteen empirical constants). Note that this burn-rate equation is computationally coupled with the equation of state $p = p(\rho, I, W)$. Elastic-plastic strength of solid material is taken into account with von Mises yield criterion to compute S_{RR}, S_{ZZ}, and S_{RZ} (note μ = shear modulus). Other options are also available, including heat conduction, other burn models, and real viscosity[7].

Only two coordinate systems ((X, Y), (R,Z)) are applicable in 2DE, namely, the slab ($\alpha = 1$) and cylindrical ($\alpha = 2$) geometry. Co-planar computation (as in our interround problem) can be treated with circular input[8]. To set up a given problem for 2DE computation, we first divide the flow field into a number of rectangular regions according to the problem configuration. Each rectangle is again divided into cells, and the total number of cells (as IJ in Tables I-III) is determined by the chosen cell sizes ($\Delta X = X/I$, $\Delta Y = Y/J$). The time step is $\Delta t \approx \Delta X/40$. Input data (numerical or logical) are supplied for each rectangle, and the total number of computing cycles is specified. Computation is then carried out in six phases during each cycle to yield a field solution of the flow problem. The finite-difference scheme for all six phases is described in detail by Mader[7].

Let us consider the numerical solution in the form $\phi = F_i(R, Z, t)$ with ϕ = P, ρ, T, I, U, V, and W ($i = 1, 2, \cdots$). Using computer graphics, we can now generate many plots to describe the reactive flow in one (1D), two (2D), and three (3D) dimensions. Thus, we can have 3D plots, $P = F_1(R, Z)$ with t = constant and $P = F_2(Z, t)$ with R = constant. Isobars are 2D plots, $F_3(R, Z) = 0$ with P, t = constant. Useful 1D plots may be $P = F_4(Z)$ with R, t = constant, $P = F_5(t)$ with R, Z = constant, and $P = F_6(R)$ with Z, t = constant. All these plots are merely snapshots or histograms. Likewise, computerized movies (3D, 2D, 1D) can be produced by letting t vary with R and/or Z.

B. Application to NOL Gap Test

We ran a sample calculation of the NOL gap test prior to the application of the 2DE code to our numerical experiments on shock sensitivity of munitions. A sketch of the NOL large scale gap test (LSGT) configuration as used in the computation is shown in Figure 3. In this example VTQ was the test propellant, and we set up the problem with 40 X 140 = 5,600 cells. We chose $\Delta R = \Delta Z =$ 1.826 mm and $\Delta t = 0.05$ µsec. To account for the material strength of Plexiglas, we also included an elastic-plastic grid of 30 X 35 = 1,050 cells. All material constants were taken from Reference 9. The problem was run in cylindrical geometry for 440 cycles, and our computed results for the shock initiation of VTQ with 36.5 mm gap are shown as contour plots in Figures 4 and 5. Note that these check with Bowman's results[9] for 40.2 mm gap consistently. For complementary details, see Reference 9.

C. Application to Munitions Problem

Since the major events of interest to us occur in an almost coplanar configuration as in Figure 2, a two-dimensional numerical simulation is justified. Thus, we ran our munitions problem in slab geometry with circular input and with elastic-plastic strength effects considered. In Tables I - III, we specify in the first three or four columns all types of munition problem for solution, and the remaining columns describe briefly the computational scheme with parameters already explained in Section II.A. It should be remarked that we modelled the detonation of the donor explosive (composition-B) using a C-J volume burn and that of the acceptor charge (PBX-9205) using the Forest Fire burn. These models of explosive burn[7] differ in that the former represents a steady-state detonation with an infinite rate of energy release whereas the latter is a non-steady shock buildup with a finite release rate, which may or may not develop into a complete detonation. For the purpose of shock-loading analysis, we considered an inert acceptor with most of its input data identical to those of a reactive acceptor, except that no Forest Fire burn was included. By comparing the inert and reactive results, we can gain a better understanding of the mechanism or factors which control the shock initiation processes in our problem. As listed in Tables I - III, most of the computations were performed to treat detonation phenomena with $R/R_o \leq 2$ and $N\Delta t \leq 50$ µsec. These values are smaller than those associated with the fragmentation of the donor cylinder. Since the 2DE code has no provision to compute fracture of solid material, we terminated our computations before fragmentation would have occurred.

Here a remark should be made regarding the limitations of our computations. The use of slab geometry with circular input is a practical approximation to the real axi-symmetric cylindrical problem. The choice of casing thickness was rather limited, since at least four cells are needed to smear shock waves with artificial viscosity. A practical lower limit on cell size is provided by the consequent short time step or large number of computing cycles as well

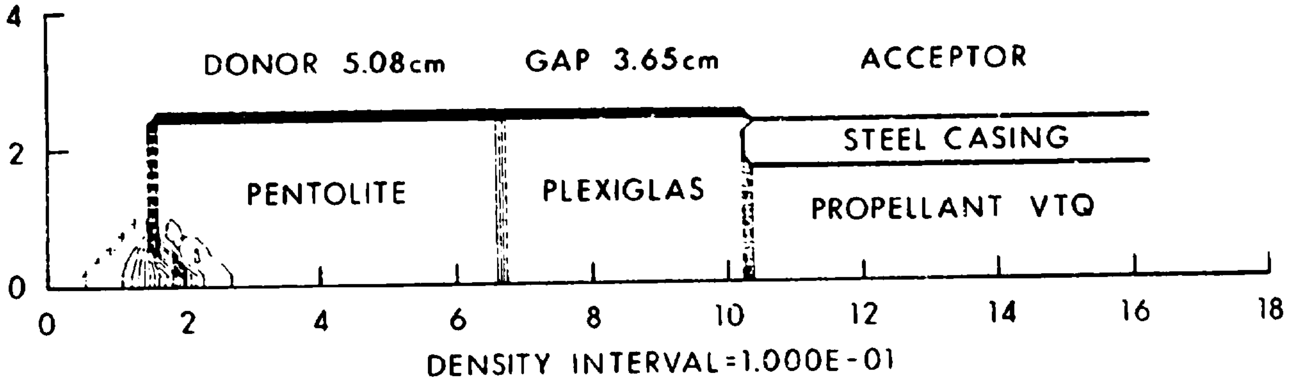

Figure 3 - Computational Sketch of NOL Gap Test

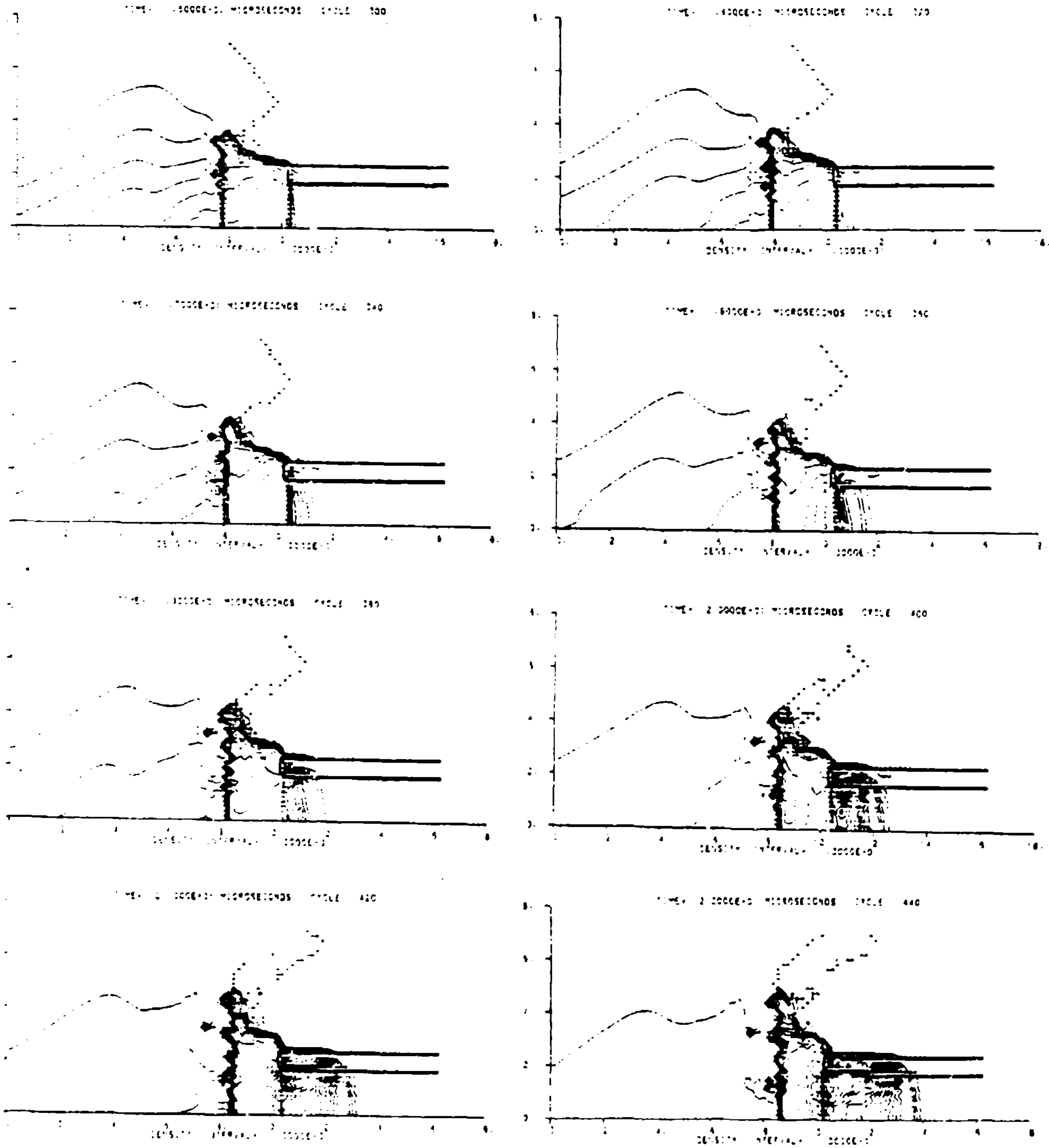

Figure 4 - Density Contours for NOL Gap Test

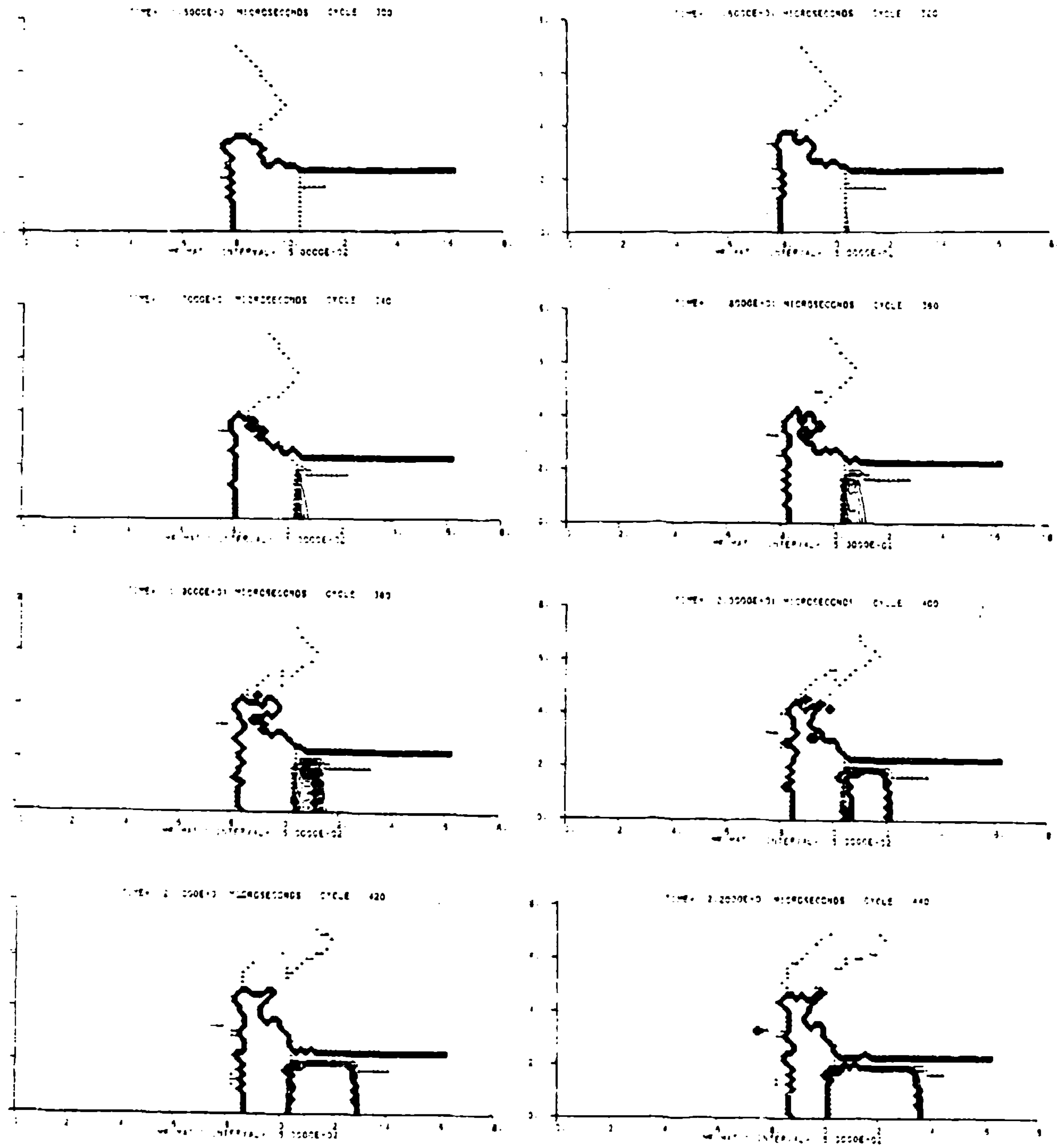

Figure 5 - Mass Fraction Contours for NOL Gap Test

as by the large computer memory required. For these reasons we used only r/R_o = 0.15 for thin-walled cylinders. Mixed-cell computation of 2DE code and boundary irregularities are still far from adequate.

III. RESULTS AND DISCUSSION

A. Flow and Shock Patterns of Interactive Munitions

1. Reactive Flows within Donor and Acceptor.

Our twenty computations indicate two distinct types of reactive flow within the donor and acceptor. Once detonation is initiated from the donor axis, diverging and converging cylindrical shocks reverberate in both the gaseous detonation products and steel casing. The shock reverberation varies considerably with the parameters R/R_o, r/R_o, and h/R_o. Another kind of reactive flow is generated in the acceptor. This flow is non-cylindrical, diverging, and shock-induced. The threshold of shock initiation appears to be of the order of the large scale gap test 50% point. It is the shock buildup that shapes the contour of this flow. Shock loading is not only complicated but also different in the two casings. Concentric cylindrical shocks reverberate in the donor casing, whereas only diverging, curved shocks advance in the acceptor casing from one side to the other - sometimes resulting in a collision which sends backward running shock in the explosive. For R/R_o = 1.5 and 2.0, air shocks are felt by the acceptor casing and explosive. However, they are insufficient to cause reaction.

2. Propagation of Reactive and Inert Shock Waves.

The above observations are common to all the types of problems we have studied (see Tables I - III). In particular, let us refer to cases A-1, A-1n B-1, B-1n, C-1, and C-1n. Figures 6 - 11 give their shock profiles plotted as $P = F_2$ (X, t) along the axis Y = 0. These plots are complementary in pairs (reactive versus inert acceptors). Thus, Figures 6 and 7 show the same diverging-converging flow on the donor side, but the propagative responses differ on the acceptor side depending on shock sensitivity. In the donor explosive, a C-J detonation begins as a spike of 28 GPa, spreading with a steady wave front of 17 GPa (note that cylindrical divergence causes this reduction of 11 GPa in the first microsecond). This steady detonation front advances with a straight-line trajectory in the Xt-plane (i.e., dX/dt = detonation velocity). About 5 μsec later the detonation front is reflected from the steel casing, and shock transmission and reverberation occur in the casing with pulses as labelled in Figure 7. A reflected shock in the detonation products converges inward and then diverges outward, upon reflection, like a second explosion. (The converging shock with a peak pressure of 27 GPa diminishes rapidly at first and then slowly to 1.5 GPa.) Shock transmission to the acceptor (reactive or inert) is as follows. In Figure 6, transmitted shocks accelerate as soon as their amplitudes exceed the threshold of the LSGT 50% point. The spread of initiation and

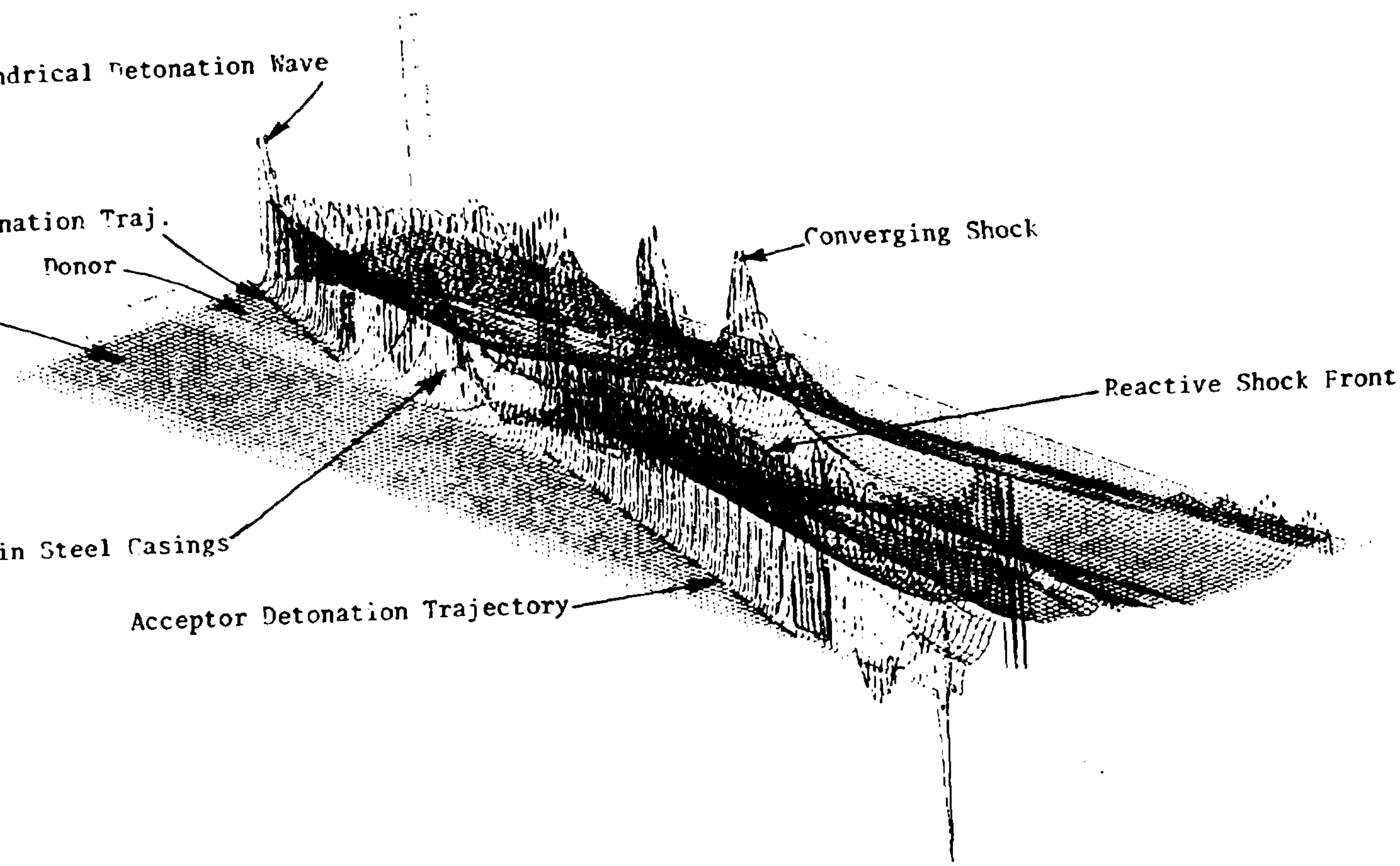

Figure 6 - Shock Pressure versus Distance and Time for Two Rounds in Contact (Reactive, $R/R_o = 1.0$)

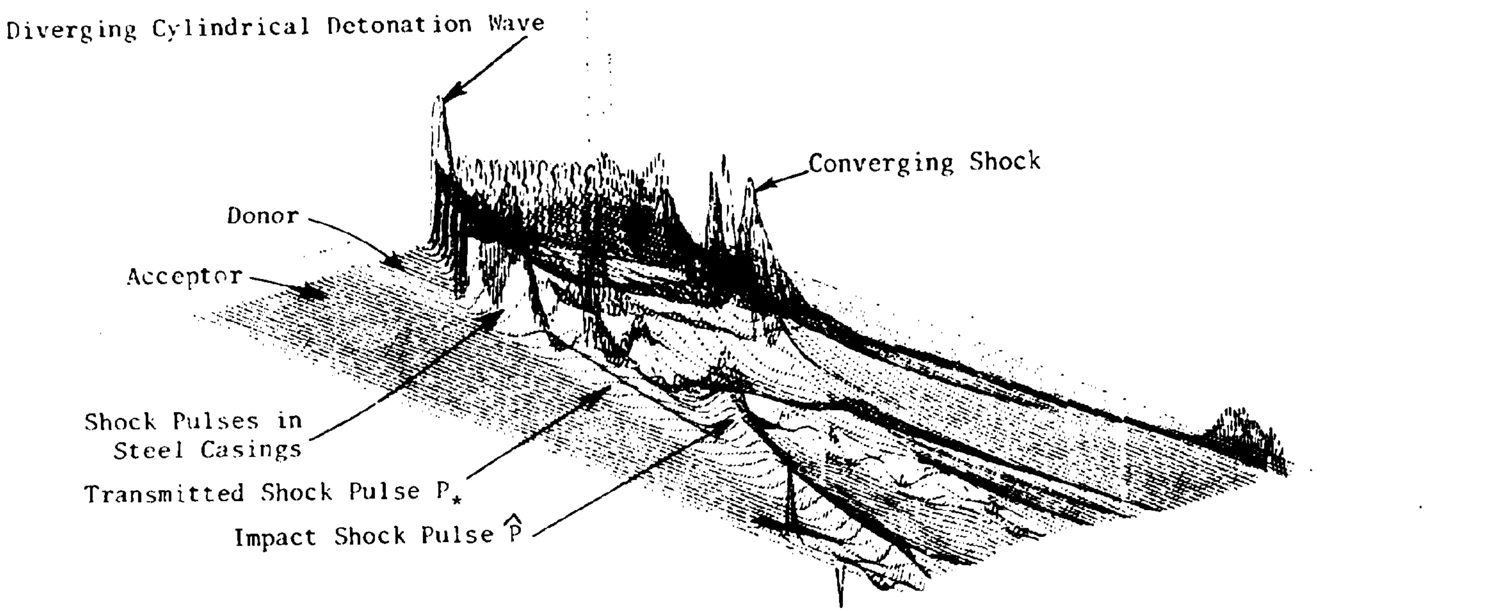

Figure 7 - Shock Pressure versus Distance and Time for Two Rounds in Contact (Inert, $R/R_o = 1.0$)

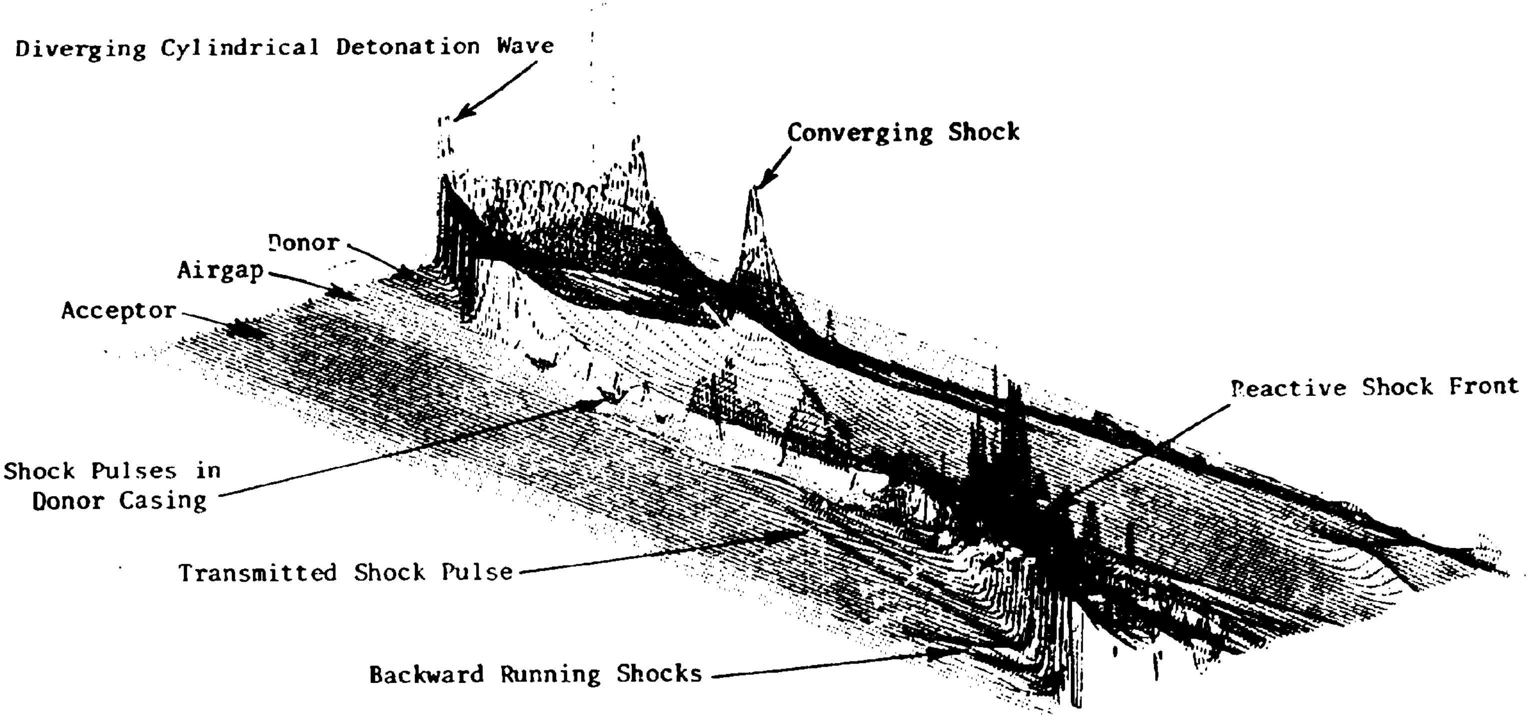

Figure 8 - Shock Pressure versus Distance and Time for Two Rounds Separated (Reactive, $R/R_o = 1.5$)

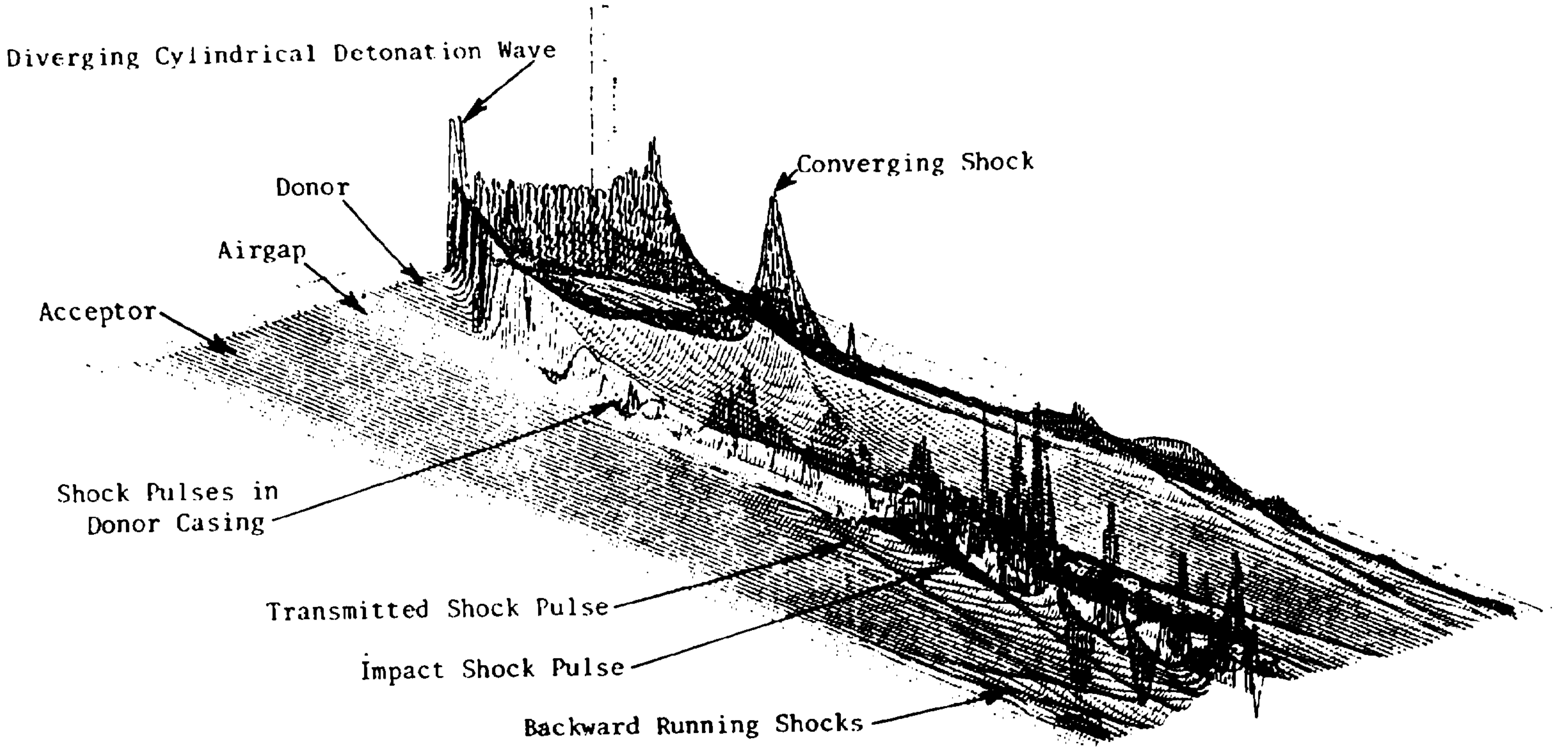

Figure 9 - Shock Pressure versus Distance and Time for Two Rounds Separated (Inert, $R/R_o = 1.5$)

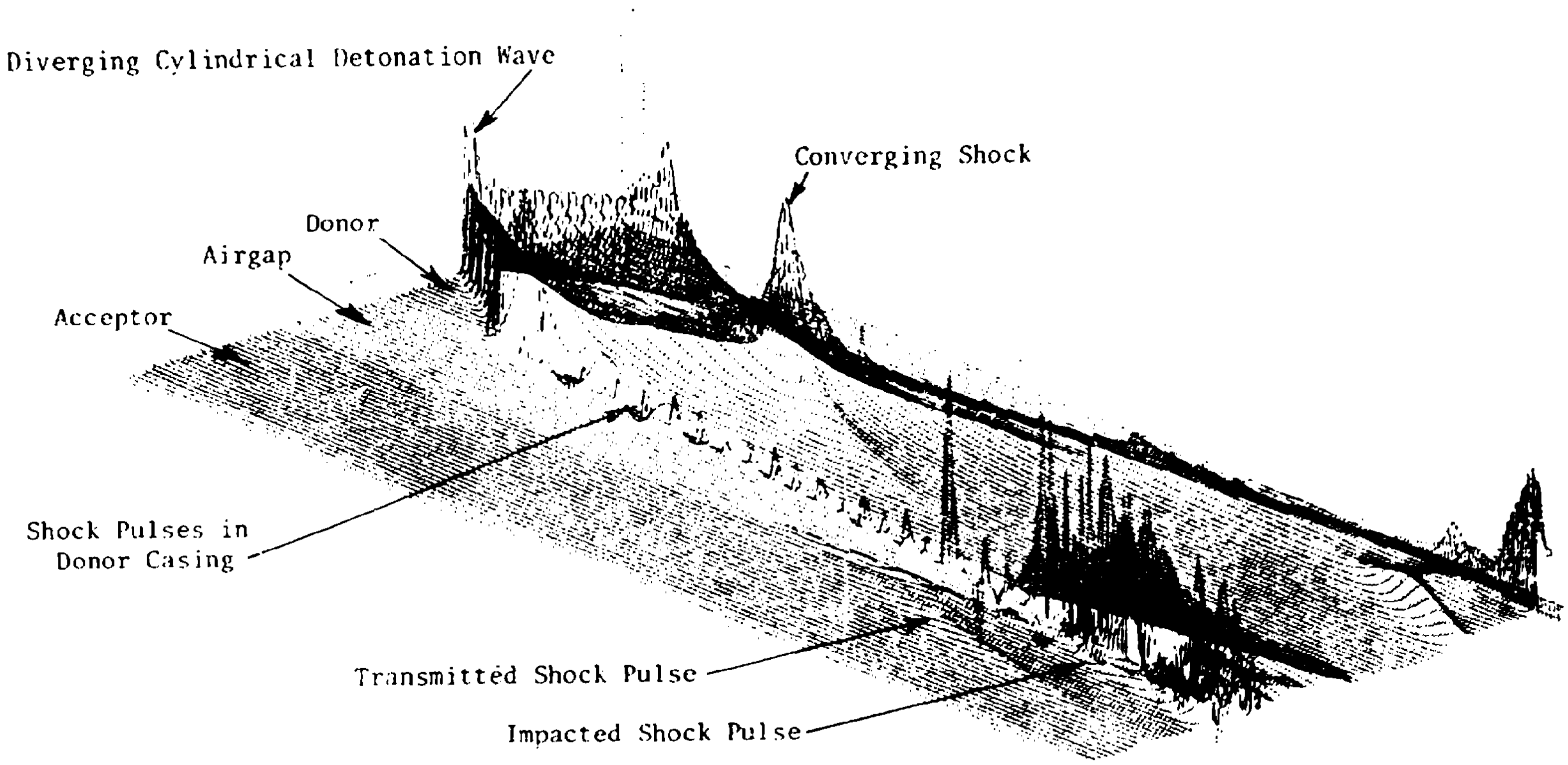

Figure 10 - Shock Pressure versus Distance and Time for Two Rounds Separated (Reactive, $R/R_o = 2.0$)

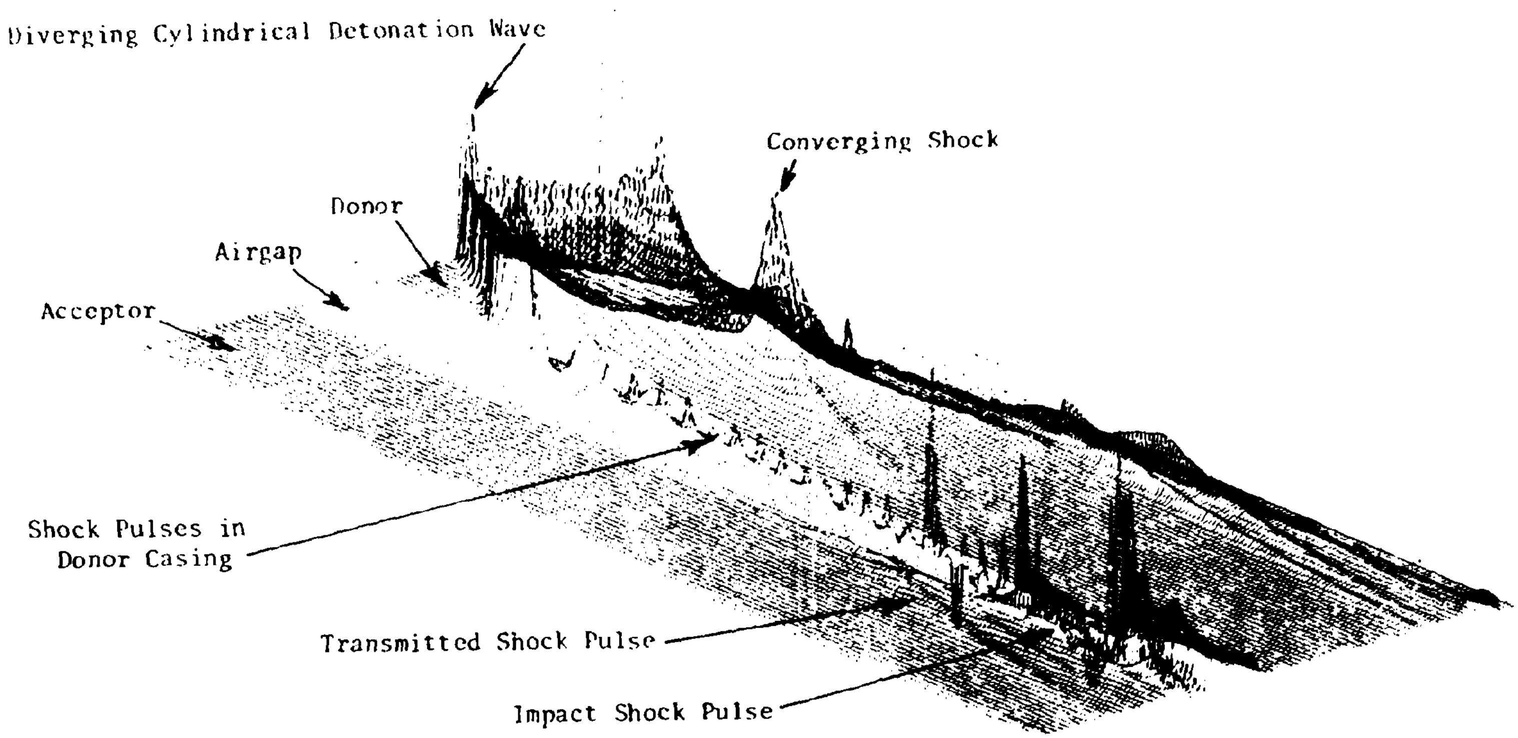

Figure 11 - Shock Pressure versus Distance and Time for Two Separated Rounds (Inert, $R/R_o = 2.0$)

reaction can be observed in Figures 14 and 15 from t = 12 μsec or cycle 240 on. The reactive shock in the acceptor builds up to the C-J state (28 GPa) at t = 16 μsec when the converging peak occurs in the donor gases (see Figures 12 and 14). We note that this shock front also describes a straight trajectory in the Xt-plane of Figure 6. On the other hand, Figure 7 clearly shows the penetration of shocks in the inert acceptor - stronger shocks catching up the early transmitted shocks.

As in Figures 6 and 7, the reactive flow and shock waves on the donor side are the same in Figures 8 - 11. In these four problems, the air gap delays the propagation of reaction or shock waves. Such prolonged communication furnishes us with a clear picture of: (a) air shocks picked up by the acceptor casing and explosive as shown in Figure 8, (b) different shock transmission to the inert acceptor of Figure 9, and (c) shock pulses modulating in the donor casing of Figures 10 and 11. Initiation of the acceptor explosive in these problems occurs as the shock caused by casing impact builds to detonation as shown in Figures 8 and 10.

Computations A-1n, B-1n, and C-1n were performed in the same way as A-1, B-1, and C-1 except that no reaction was permitted in the acceptor. A comparison of these results enables us to distinguish between the inert and reactive responses of an acceptor to the same shock stimuli. Such a comparison is useful to assess the shock sensitivity of the simulated munition and the factors which control the shock initiation of the acceptor.

A close look at Figures 6 - 11 indicates that early transmitted shocks cause no significant reaction in the acceptor. In all cases of reactive communication, initiation occurs in the acceptor as a result of shock buildup either by the donor's converging-diverging flow with $R/R_o = 1.0$ (see Figure 12 for A-1, A-2, and A-3 beyond distance = 15 cm) or by casing impact upon closing the air gap with $R/R_o = 1.5$ and 2.0. Note that the impact shock pulses all have peaks exceeding the LSGT 50% point. As already noted, the converging-diverging shock occurs in the donor as if it were a second explosion. Figure 12 shows the timing and amplitude of this shock from a matrix of nine computations. We see that both the amplitude and time of occurrence decrease as the casing thickness increases. These will affect the initiation of the acceptor explosive. As depicted in Figure 13, a converging shock can also be formed in an inert acceptor. Note that Figures 12 and 13 are both 1D plots of $P = F_4(X)$ along the axis Y = 0 and at specified times.

3. Description by Contour Plots.

Both isobar and mass-fraction contour plots show the reactive flows and shock waves with greater clarity. Without indicating the pressure levels, we note that the sixteen isobar plots of Figure 14 show the C-J spike clearly (in cycle 1), the diverging cylindrical detonation front, reflected shocks, the converging shock (in cycle 320), and the prolonged expansion of the detonation products and donor casing. The initiation, buildup, and propagation of detonation in the acceptor explosive from cycle 240 to 480 are shown in both Figures 14 and 15. Note that here the reactive shock is diverging

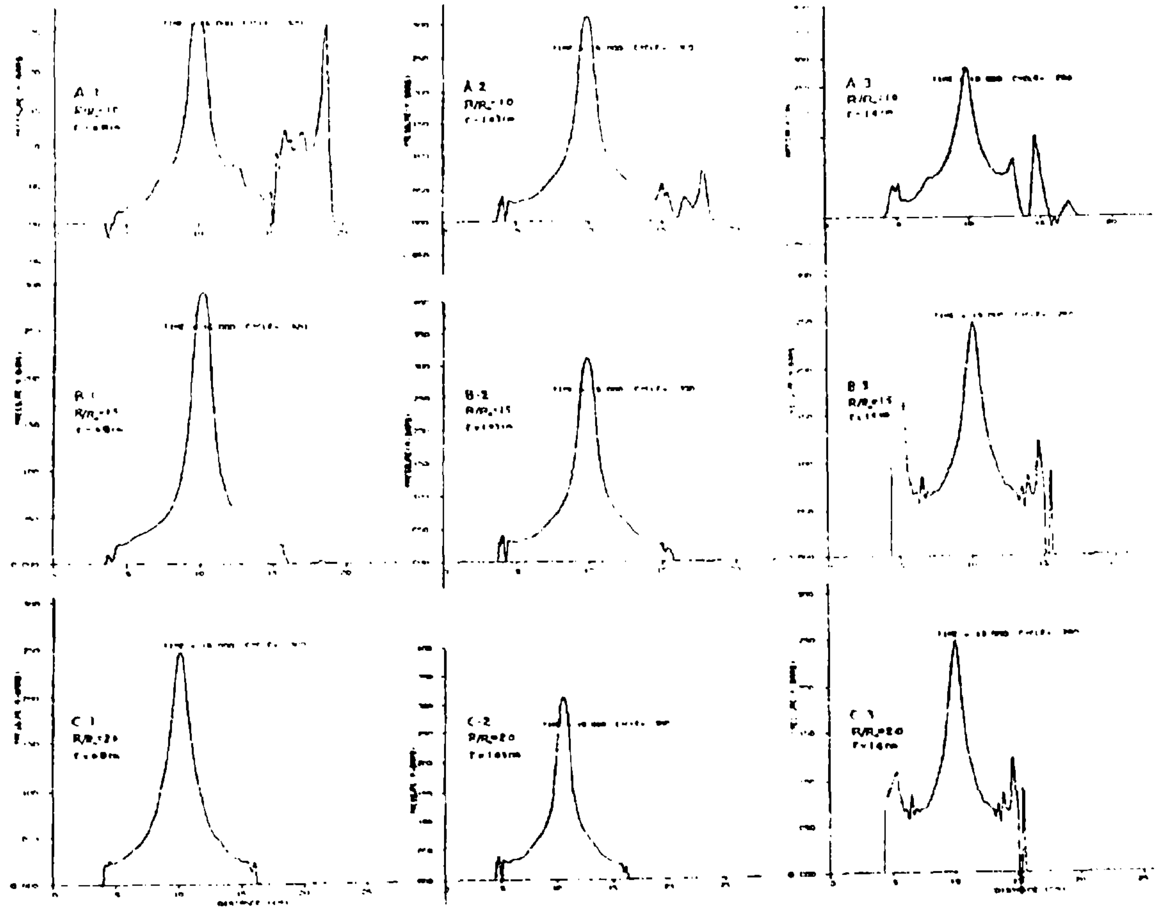

Figure 12 - Converging Shock Profiles in Donors with Various Separation and Casing Thickness

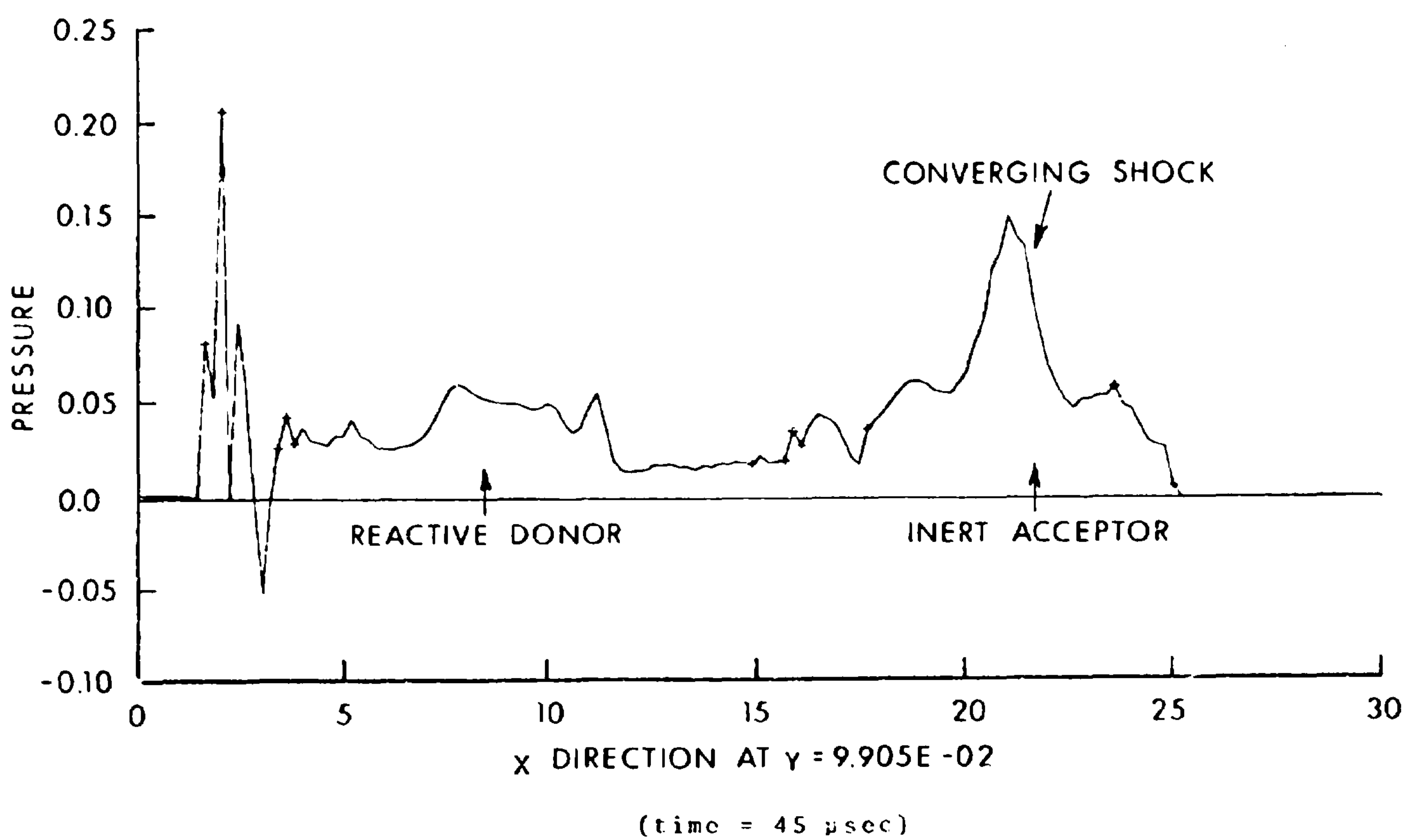

Figure 13 - Converging Shock Formed in Inert Acceptor with $R/R_o = 1.0$ and $r/R_o = 0.27$

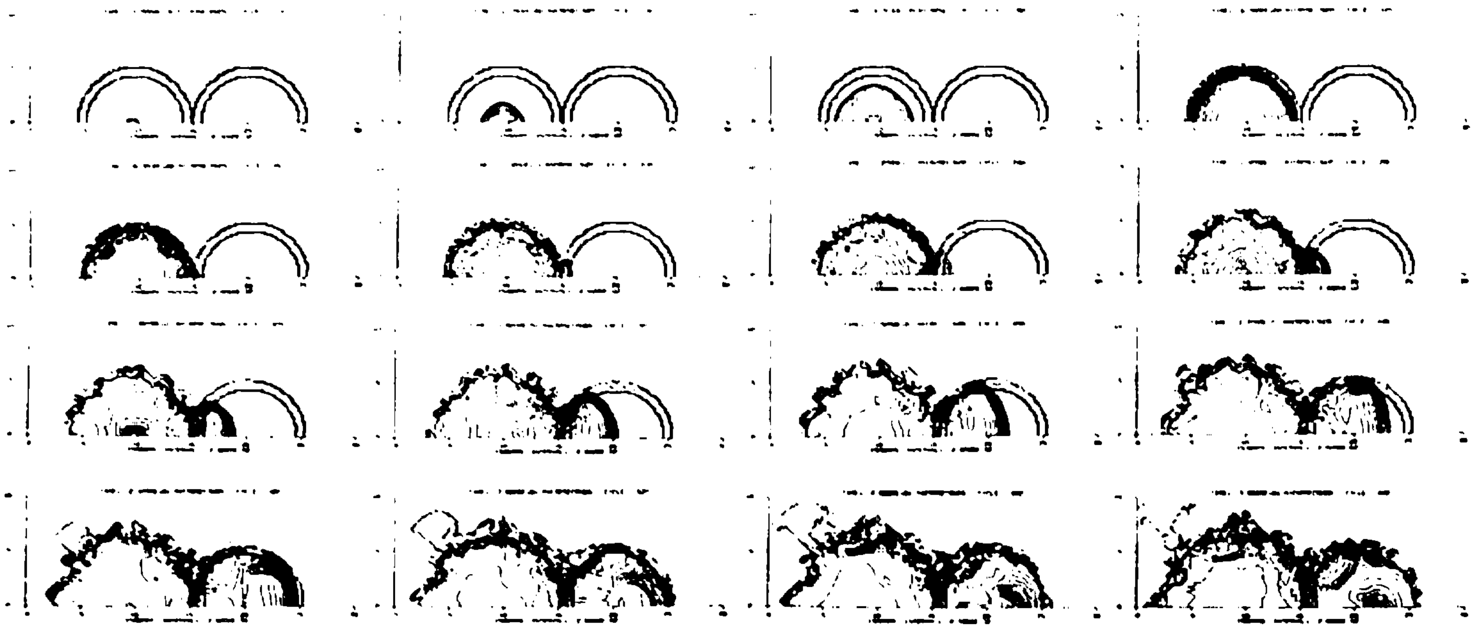

Fig. 14 - Isobars of Two Rounds in Contact (Reactive, $R/R_o = 1.0$)

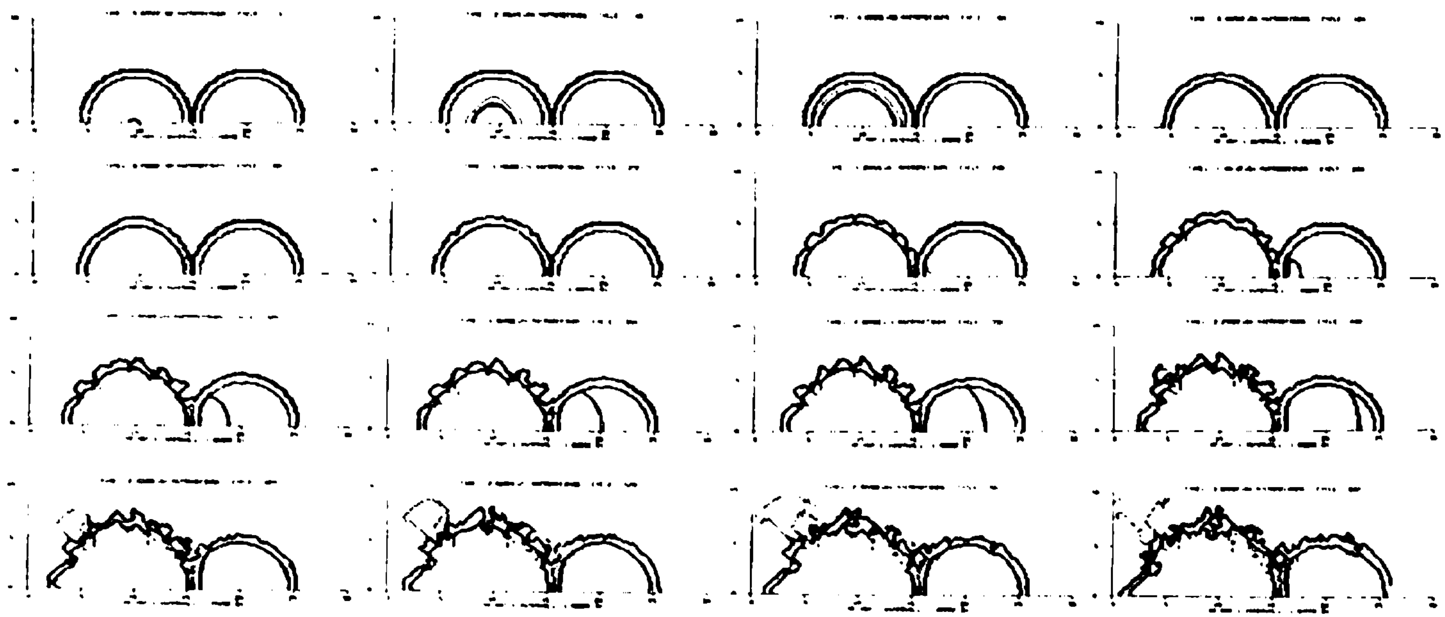

Figure 15 - Mass Fraction Contours of Two Rounds in Contact (Reactive, $R/R_o = 1.0$)

(although not cylindrical) and advances with decreasing curvature (increasing strength). This may be attributed to the heavy confinement on one side and the Taylor rarefaction on the other. There is appreciable shock transmission from the acceptor back to the donor. Note also that an eccentric converging shock forms within the acceptor (see Figure 14, cycle 600) as a result of the detonation propagation and reflection (see Figure 14, cycles 480, 520, 560, and 600). The irregular shape of the donor casing in Figure 15 is a combined result of a circular boundary described in rectangular coordinate and mixed-cell computations. Of course, this is not the true deformation as sketched in Figure 16 which shows a superposition of two rounded-off contour plots.

B. Response of Reactive Acceptors

1. Shock Initiation.

Shock waves penetrating into the acceptor explosive compress it and generate hot spots which may multiply and cause significant reaction. A complete buildup to detonation presumably depends upon either a critical incipient energy[10] or certain reaction rate. In 2DE code computation this rate is given by the Forest Fire burn[7] as an exponential function of shock pressure only. On the basis of a single buildup, the Forest Fire model is constructed for heterogeneous shock initiation as represented by the Pop plot generated from wedge-test results (note that one-dimensional shock sensitivity data are used here in the same way that 1-D shock Hugoniots are used in the HOM equation-of-state computations, i.e., without considering multidimensional effects). Accordingly, the computation of the Forest Fire burn rate is an essential part of 2DE modeling of our interround detonation phenomena. Figure 17 depicts a heterogeneous shock initiation trajectory Od in the Xt-plane as obtained from a wedge test. The initial slope of this trajectory is equal to the initial shock velocity and the final slope is equal to the CJ-detonation velocity (curve od being tangent to straight line dD along which proceeds steady-state detonation). To simplify the description, let us consider chord od with $U_a = X_d/t_d$, the average velocity of shock buildup (see the insert in Figure 17), where X_d is the distance to detonation and t_d the time to detonation. The parameter U_a increases with the strength of the shock stimulus or the sensitivity of the explosive ($U_a \leq D$, D being CJ-detonation velocity). Conversely, tardy responses correspond to small values of U_a as in acceptors with thick casings or at large distances of separation (see Figures 24 and 25).

2. Effects of Parameter Variations.

Shock initiation of the acceptor explosive may be influenced by many factors. Here we consider those parameters which are obtainable from our 2DE computations. In Table IV we list values of such parameters, including our notations and symbols.

---

[10] *Walker, F. E. and Wasley, R. J., "Critical Energy for Shock Initiation," Explosivestoffe 17, 9 (1969). See also the Sixth Symposium (International) on Detonation, ACR-221 (1976) for several discussions on this topic.*

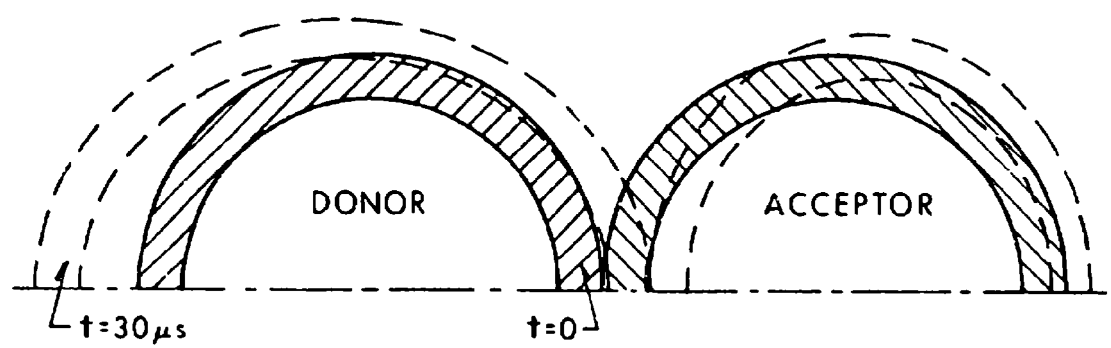

Figure 16 - Sketch Show' g Deformation of Two Rounds in Contact (Reactive, $R/R_o = 1.0$, $r/R_o = 0.15$)

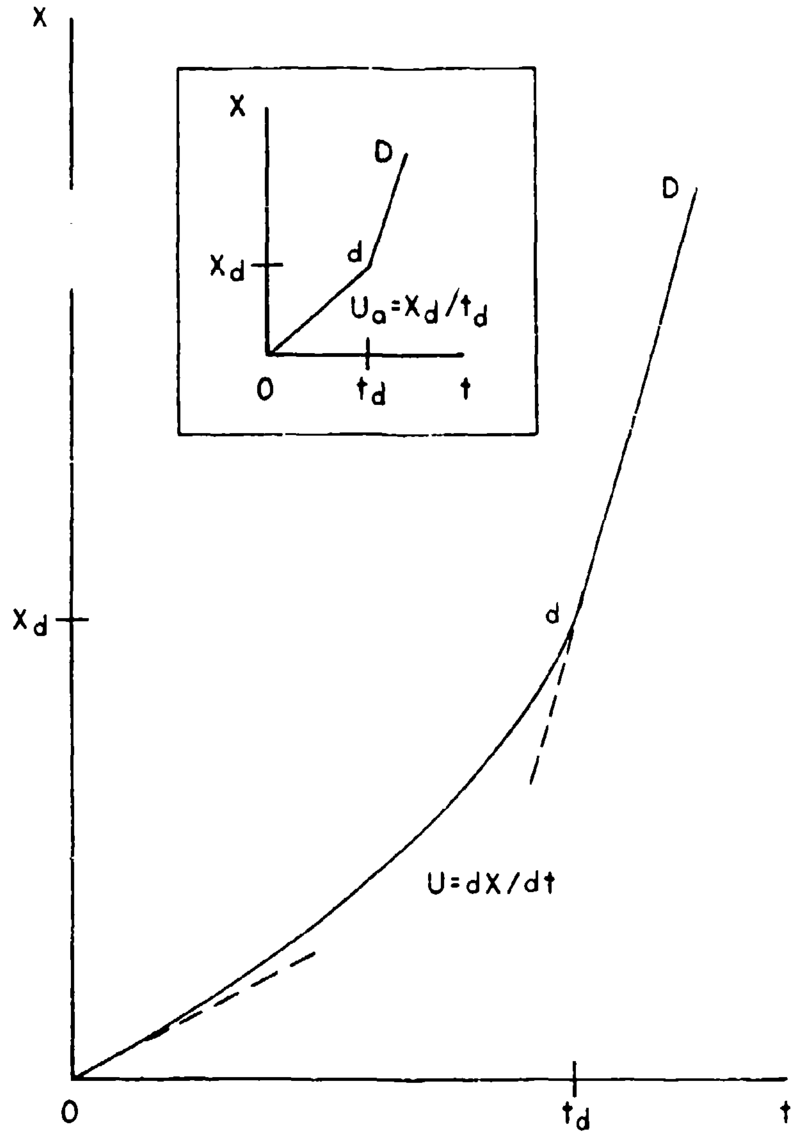

Figure 17 - Schematic of Shock Trajectory for Heterogeneous Initiation Process

TABLE IV

SHOCK INITIATION RESULTS

Case	R/R_o	r/R_o	t_1/t_c	P_1	t_2	P_2	t_3	P_3	t_r	t_d	X_d	U_a	P_i
A-1	1.0	0.15	9	0.7	12	5.0	15	24.0	3	6	25	4.2	2.93
B-1	1.5	0.15	17/29	0.2	32	4.0	35	25.0	3	6	23	3.8	3.10
C-1	2.0	0.15	25/37	0.1	42	4.0	47	25.0	5	10	27	2.7	2.78
A-2	1.0	0.20	9	0.5	13	5.0	18	24.0	4	9	38	4.2	2.22
B-2	1.5	0.20	19/30	0.1	35	5.0	38	25.0	5	8	27	3.4	2.78
C-2	2.0	0.20	27/39	0.1	46	4.0	52	25.0	7	13	32	2.5	2.48
A-3	1.0	0.27	11	0.8	20	5.0	25	25.0	9	14	45	3.2	1.98
B-3	1.5	0.27	19/31	0.1	-	-	-	-	-	-	-	-	-
C-3	2.0	0.27	28/40	0.2	-	-	-	-	-	-	-	-	-

Note: B-3 and C-3 computation terminated too early to yield all data..

Symbols and Notations:

t_1 = time when first shock enters the acceptor explosive

t_c = time of casing contact

t_2 = time when significant reaction occurs ($P_2 \approx$ LSGT 50% point)

t_3 = time approaching CJ-state ($P_3 \approx P_{CJ}$)

t_r = time of shock run to significant reaction, μsec

t_d = time to detonation, μsec

$t_r = (t_2 - t_1)$ or $(t_2 - t_c)$, μsec

$t_d = (t_3 - t_1)$ or $(t_3 - t_c)$, μsec

$x_d = x_3 - x_1$, mm

$P_i = \left(x_d\, e^{-A}\right)^{1/B}$, GPa

With D and P_{CJ} denoting the CJ-detonation velocity and pressure respectively, we also introduce $t_o = R_o/D$ as a characteristic time for the reactive acceptor. Now we can normalize all initiation parameters of Table IV and plot the results as shown in Figure 18 - 25. Each of these plots may be looked upon as an expression of the form:

$$\eta_i = f_i \ (R/R_o, \ r/R_o, \ h/R_o, \ \xi \ ) \qquad (10)$$

where η_i (i = 1, 2,...) are response parameters, say, $\eta_1 = t_r/t_o$, $\eta_2 = t_d/t_o$,..., and ξ is an explosive parameter implicitly held constant here. We are interested in the general trends exhibited in these plots rather than in their analytic expression such as Equation (10).

It is worth noting that all curves in Figures 18 and 19 have a trend of increasing reaction delay as the casing thickness or interround separation is increased. Specifically, we observe in Figure 19 greater reaction delay with $r/R_o > 0.2$ than with $r/R_o < 0.2$ for $R/R_o = 1.0$. In Figure 18 we note little delay with $1.0 < R/R_o < 1.5$ but considerably greater delay with $1.5 < R/R_o < 2.0$ for $r/R_o = 0.15$.

In Figures 20 and 21 a similar trend is shown using the time required for shock buildup to detonation. A comparison between Figures 18 and 20 reveals that for $r/R_o = 0.2$ a change of R/R_o from 1.0 to 1.5 results in a reaction delay (Figure 18) but an advance of full detonation (Figure 20). It is also interesting to note that in Figure 21 the difference between R/R_o = 1.0 and 1.5 is narrow down with $0.15 < r/R_o < 0.20$. A similar trend exists between R/R_o = 1.0 and 2.0 with $0.20 < r/R_o < 0.25$.

The initiation parameter X_d was taken as the distance traversed by the reactive shock front along the symmetry axis during buildup to detonation. It was then used as a simple one-dimensional model for computing $U_a/D = X_d/Dt_d$ and $P_i/P_{CJ} = (X_d \, \bar{e}^{A})^{1/B} / P_{CJ}$ for Figures 22 - 25, where A and B are the Pop plot constants as taken from Reference 9. Of course, the shock stimuli and buildup in our interround problems are multiple, two-dimensional waves. Here we seek only a crude representation of the initiation phenomena using Figures 22 - 25 (more realistic model not yet available). Thus, the trend of Figure 22 may be interpreted as follows. The shock stimuli are

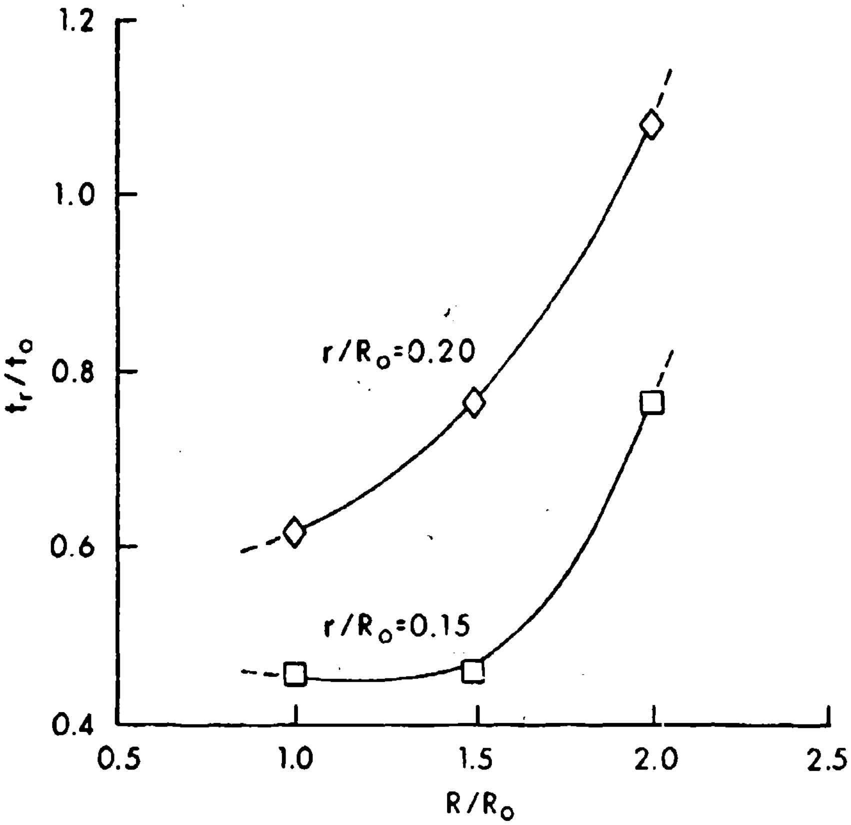

Figure 18 - Effects of Interround Separation on Time to Reaction

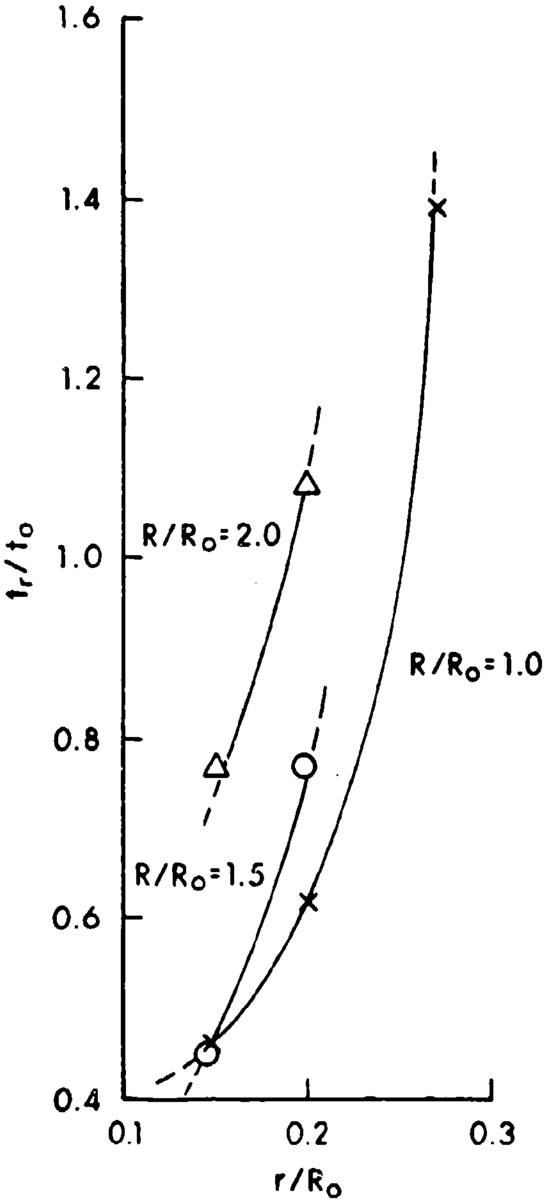

Figure 19 - Effects of Casing Thickness on Time to Reaction

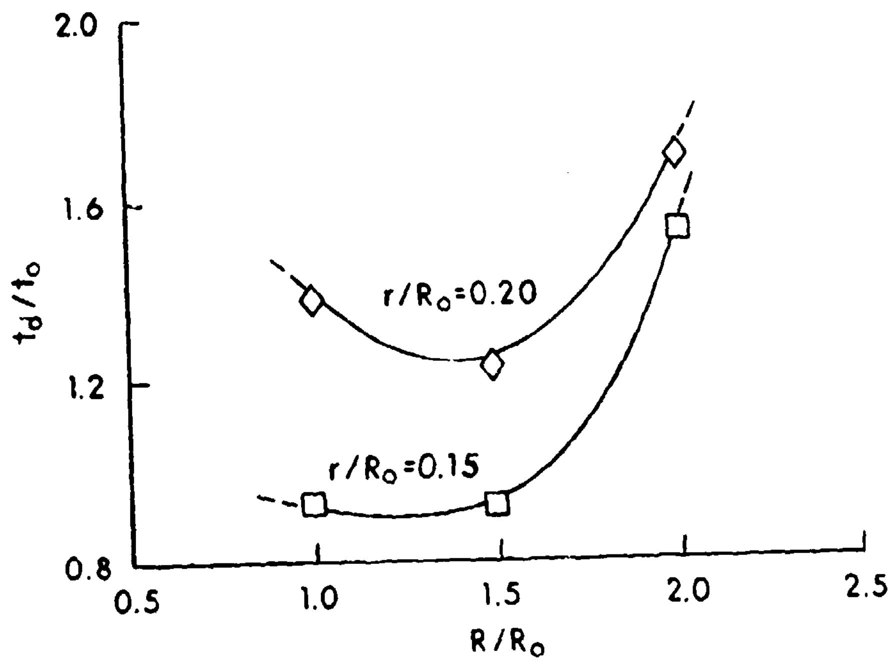

Figure 20 - Effects of Interround Separation on Time to Detonation

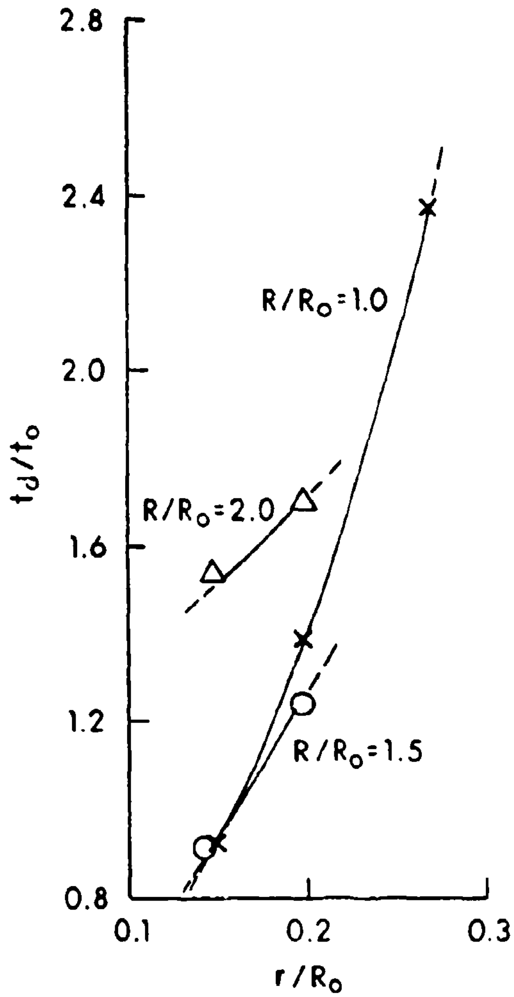

Figure 21 - Effects of Casing Thickness on Time to Detonation

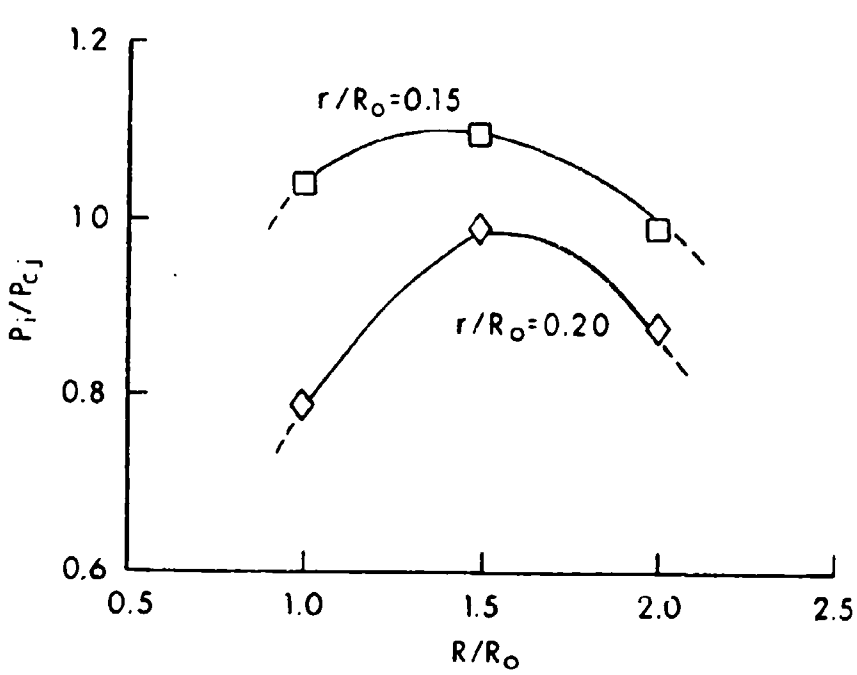

Figure 22 - Effects of Interround Separation on Initial Shock Pressure

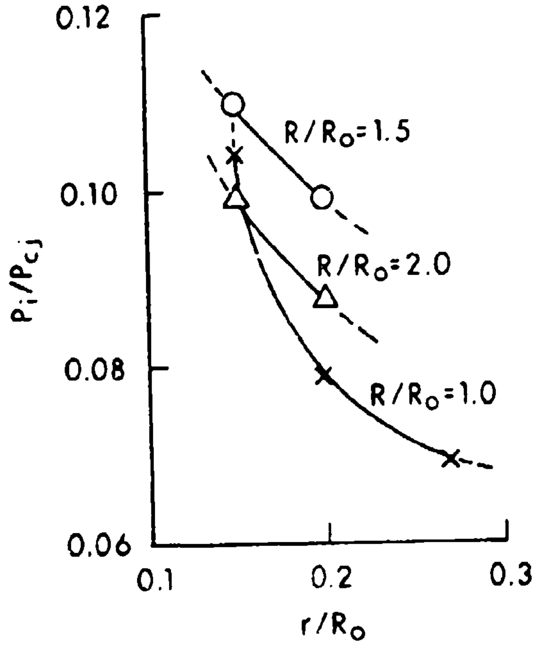

Figure 23 - Effects of Casing Thickness on Initial Shock Pressure

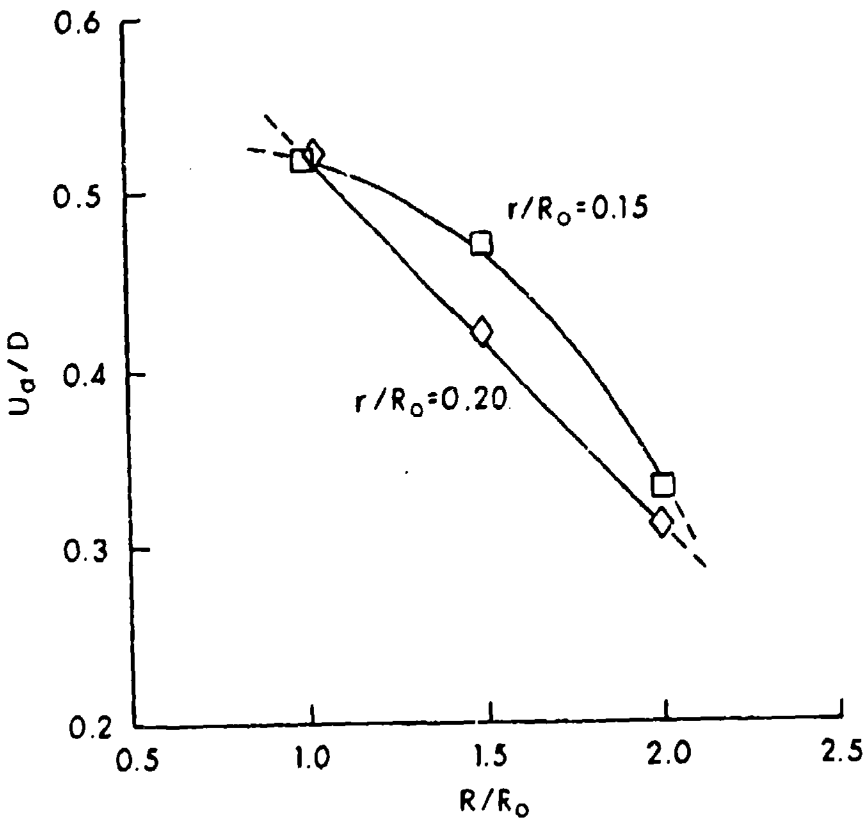

Figure 24 - Effects of Interround Separation on Average Velocity of Shock Buildup

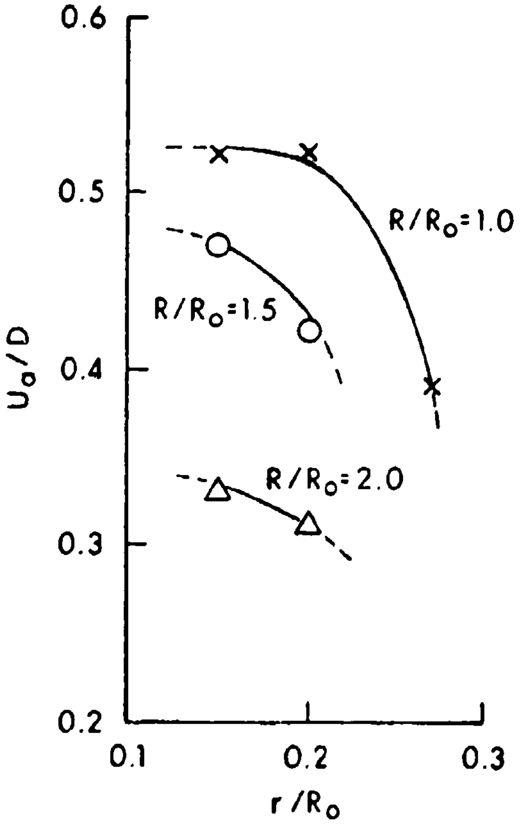

Figure 25 - Effects of Casing Thickness on Average Velocity of Shock Buildup

due to the converging-diverging cylindrical flow as if it were a second explosion in the donor with $R/R_o = 1.0$, but they derive from quite different mechansims for $R/R_o = 1.5$ and 2.0. Upon closing the air gap, casing impact deliver to the acceptor explosive shocks which coalesce as if they were stronger initial pulses for $R/R_o = 1.5$. As R/R_o increases from 1.5 to 2.0, the shock stimuli become weaker again. It is worth noting that the change in trend of Figure 22 matches that of Figure 20 consistently - more delay of detonation due to weaker shock stimuli. Within the range considered, there is a minimum delay due to the maximum stimuli at $R/R_o = 1.5$. In Figure 23, a decreasing trend is observed of shock intensity versus casing thickness. Note the relative shock intensities for $R/R_o = 1.5$, 2.0, and 1.0 at $r/R_o = 0.20$. In fact, these are due to different mechanisms of shock transmission as mentioned earlier. Both Figures 24 and 25 indicate that shock buildup is retarded either by interround separation or by casing thickness, as expected from intuition.

Using Figures 18 - 25, we have examined the effects of varying interround separation and casing thickness on shock sensitivity of munitions. A simple assessment is to determine the general trends of these figures which describe relations between dimensionless parameters. Such trends can serve as a practical guide for scaling or interpolating detonation phenomena within the range of our numerical simulation.

C. Response of Inert Acceptors

1. Shock Loading.

To check the shock loading on an acceptor explosive, we computed the dynamic response of the acceptor filled with a dummy explosive. Shock pressures were taken for the explosive cell nearest the casing as a function of time only - viz. $P = F_5(t)$ as mentioned in Section II.A. P_* refers to the peak pressure at time t_* of the transmitted shock pulse; $\hat{P}$ is the peak pressure at time $\hat{t}$ of the impact shock pulse; P_1' and P_2' are shock pressures at times t_1 and t_2 respectively as mentioned earlier (see Table V); and P^2dt is integrated over time in order to apply the critical energy criterion[10]. Note the difference between P_1' and P_* with $t_1 < t_*$. These are usually too weak to induce any significant reaction. With $t_2 < \hat{t}$, P_2' belongs to the impact shock pulse which is responsible for shock initiation whenever $\hat{P}$ exceeds the LSGT 50% point. Notably, as calculated for the inert acceptor, P_2' is more comparable with P_i than with the LSGT 50% point. But P_2 values for the reactive acceptor turn out to be just about at the LSGT 50% point (see Table IV). Such comparison is consistent with the shock buildup. Table V gives the numerical results of inert-acceptor response, with all t's in μsec and all P's in GPa.

TABLE V.

SHOCK LOADING RESULTS

Case	R/R_0	r/R_0	t_*	P_*	$\hat{t}$	$\hat{P}$	$\int P^2 dt$	t_1	P_1'	t_2	P_2'
A-1n	1.0	0.15	10.2	4.0	19.4	7.9	6.1	9	1.3	12	2.3
B-1n	1.5	0.15	23.0	0.8	35.8	6.9	7.5	17	0.07	32	1.2
C-1n	2.0	0.15	25.2	0.1	43.6	5.5	12.0	25	0.1	42	1.0
A-3n	1.0	0.27	13.2	1.1	24.2	8.6	15.0	11	0.1	20	1.3
B-3n	1.5	0.27	20.2	0.1	36.2	7.9	4.0	19	0.04	-	-
C-3n	2.0	0.27	23.8	0.07	38.6	2.3	2.5	28	0.05	-	-

It is apparent that both the inert and reactive acceptors should respond identically to equal shock stimuli which cause no initiation at all (see Figures 10 and 11 and lines C-1 and C-1n in Tables IV and V respectively). Any differences between values of Tables IV and V are due to chemical reaction which affects shock buildup, and we can check them with shock sensitivity data. In fact, the response of an inert acceptor involves a complicated pattern of shock propagation and interaction. Here we have simplified our analysis of shock loading by considering only P_* and $\hat{P}$ which are essential for detonation propagation. Below we seek to examine our shock loading results from a viewpoint which is complementary to Section III.B.2.

2. Effects of Parameter Variations.

Using the numerical results presented in Table V, we can now examine the shock behavior of inert acceptors in order to gain some insight into the problem of detonation transfer. To construct the plots of Figures 26 - 28, we have normalized the pertinent parameters with the following standard constants[9,11] for PBX-9205:

P_{CJ} = 28.1 GPa, D = 8.13 mm/µsec (γ = 2.97)

X = 50.8 mm, P_x = 5.0 GPa (LSGT 50% point)

$P_{CJ}^2 t_0$ = 5,100 $(\text{GPa})^2$-µsec

E = 0.0019 (normalized P^2t value)

[11] *Dobratz, B. M. (ed), "Properties of Chemical Explosives and Explosive Simulants," Lawrence Livermore Laboratory Report UCRL-52997 (March 1981).*

The last constant is obtained from $E = P^2t/P_{CJ}^2t_o = U\omega/D\omega_{CJ}$ with U = 3.9 mm/μsec (using P_x and shock Hugoniot to compute), $\omega = Put = P^2t/\rho_oU$ = 14.6 GPa-mm (using the value[11] for composition-B as a close estimate here), and $\omega_{CJ} = P_{CJ}R_o/(\gamma+1)$ = 372 GPa-mm.

Figure 26 shows that all shock pressures P_* and $\hat{P}$ decrease as the interround separation R/R_o increases. Using the LSGT 50% point (viz. horizontal line P_x/P_{CJ} = 0.18) as a guide, we see that the transmitted pulses P_* are too weak and the impact shock pulses $\hat{P}$ are responsible for detonation to occur in reactive acceptors. These can readily be verified by comparing Figures 6 and 8 with Figures 7 and 9 respectively. Without including P_*/P_{CJ} which is not critical here, Figure 27 describes the variation of $\hat{P}/P_{CJ}$ with r/R_o. We note first an increasing trend for R/R_o = 2.0. With r/R_o increased from 0.15 to 0.27, the shock sensitivity of a reactive acceptor at R/R_o = 2.0 will be reduced to a "no-go" level (see Figures 26 and 27).

The critical energy criterion[10] has often been used as a guide for the assessment of shock initiation. The particular constant is the shock energy per unit area, $\omega = Put = P^2t/\rho_oU$, due to plate impact in sensitivity test. Thus, we arrived at the value E = 0.0019 earlier. Using this and values of Table V, we plot the horizontal (dotted) line and curves in Figure 28 as a check of shock sensitivity according to the P^2t criterion. Thus, the horizontal line may be regarded as the initiation threshold above which we would predict "go" and below which "no go." A comparison between such prediction and our results of Table IV indicates three points of Figure 28 (viz. a', c', c) in agreement and others (viz. a, b, b') not so. Note that the separation R/R_o = 1.5 will provide the smallest chance of initiation, if a P^2t criterion is applicable. However, as noted in Table IV, initiation occurred for R/R_o = 1.5 as well, and the P^2t criterion may not apply here.

D. Effects of Plastic Shield between Rounds

It has been shown elsewhere[1,5] that plastic shields between rounds were able to suppress detonation transfer, provided their thickness and spacing were adequate. We pursued a numerical study with values of the shield thickness, h = 10, 15, 20 and 25 mm, for R/R_o = 1.5 and r/R_o = 0.20 (see Table III). Our numerical results are given in Table VI, including D-0 which is in fact B-2 of Table IV, and D-5 for the thinnest shield considered here. We have confined our attention to R/R_o = 1.5 and r/R_o = 0.20 (see Figures 22 and 24 for the

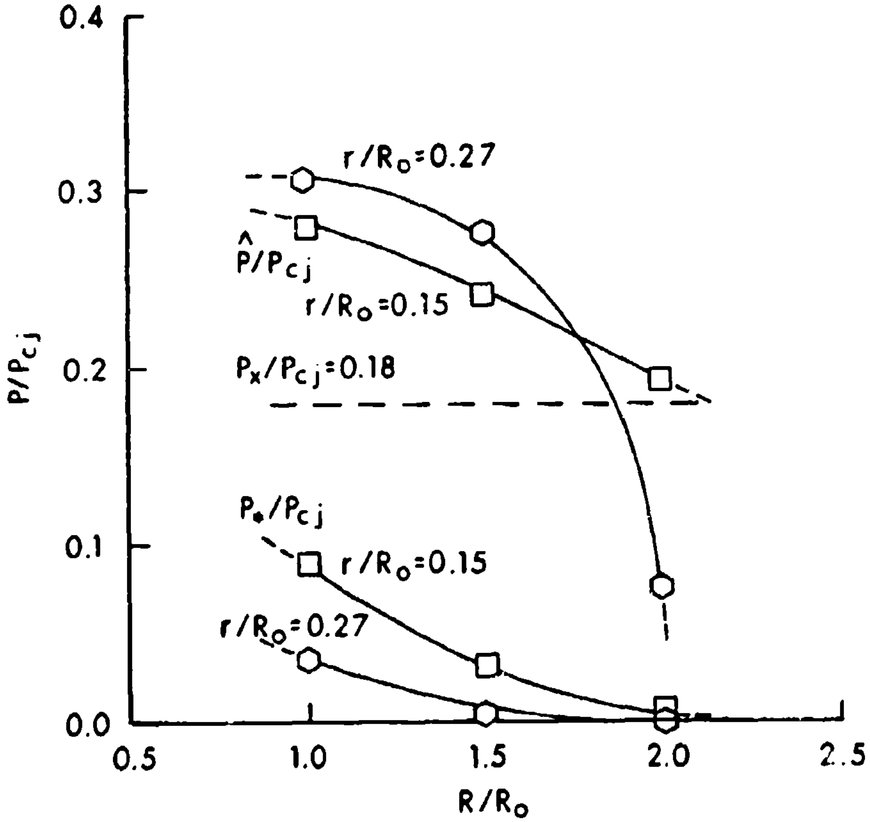

Figure 26 - Effects of Interround Separation on Inert Shock Loading

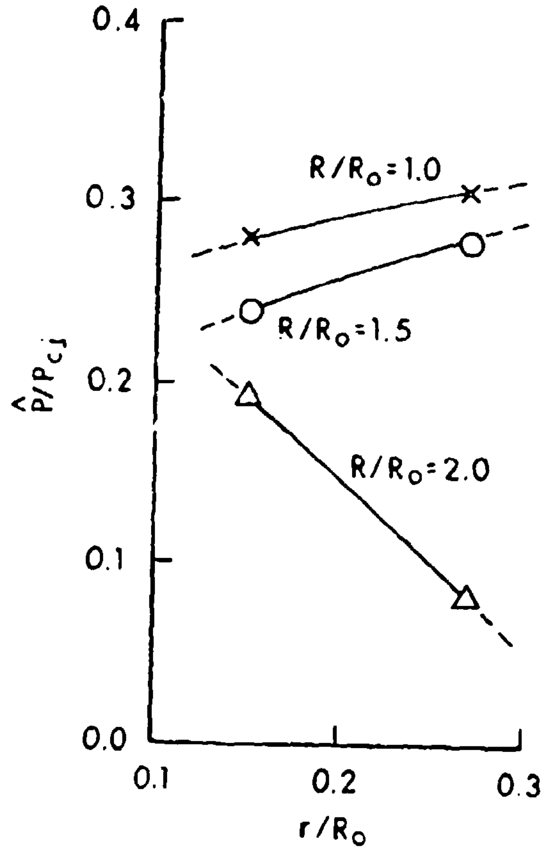

Figure 27 - Effects of Casing Thickness on Inert Shock Loading

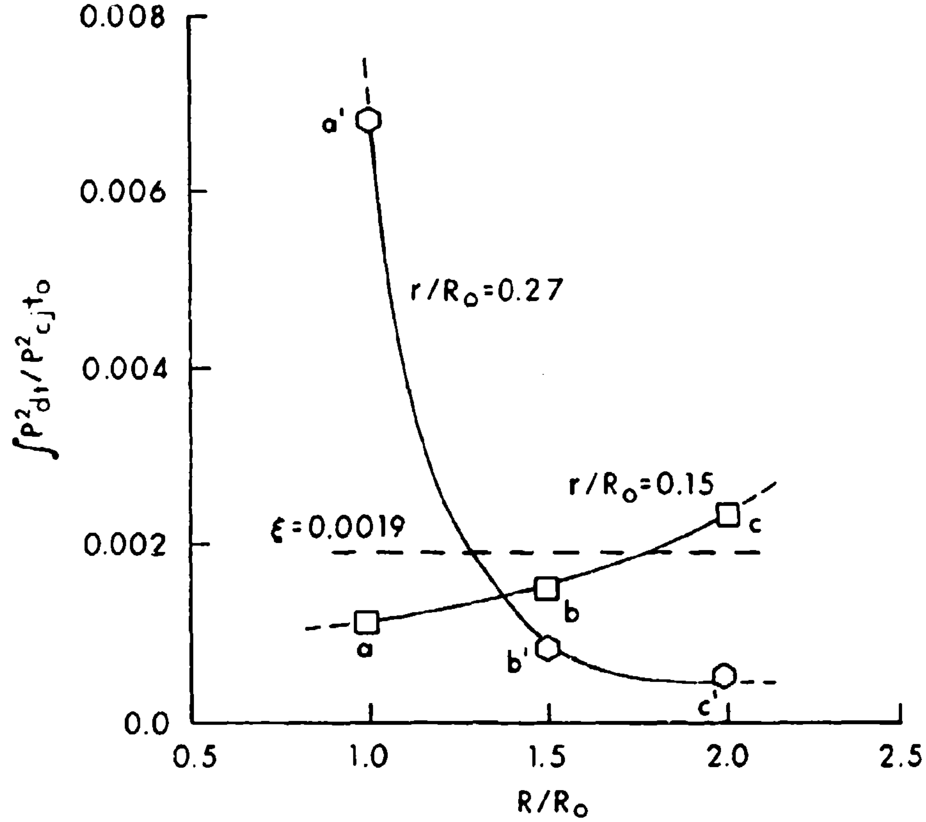

Figure 28 - Inert Response Measured with P^2t Criterion

TABLE VI

SHOCK INITIATION RESULTS WITH PLASTIC SHIELD

Case	h/R_o	t_1/t_c	P_i	t_2	P_2	t_3	P_3	t_r	t_d	X_d	U_a	P_i
D-0	0	19/30	0.1	35	5.0	38	25.0	5	8	27	3.4	2.78
D-1	0.20	19	0.4	32	3.0	-	-	13	-	-	-	-
D-2	0.28	22	0.2	29	3.0	-	-	7	-	-	-	-
D-3	0.38	20	0.3	28	3.0	-	-	8	-	-	-	-
D-4	0.47	17	1.0	26	3.0	33	28.0	9	16	22	3.5	3.19
D-5	0.14	21	0.4	29	3.0	32	35.0	8	11	28	3.2	1.96

Note: D-5 with $r/R_o = 0.15$, all others with $r/R_o = 0.20$ (See Table III).
D-1, D-2, D-3 computations terminated too early.
All t's in μsec, P's in GPa.

reduction of P_i and U_a respectively). In Figure 29 is plotted the only complete set of data on a normalized basis. Unfortunately, almost all computations terminated early. With six data points, we obtained an N-shaped curve describing the effect of increasing shield thickness from one extreme value to the other. It is interesting to note the increase of t_r/t_o in Figures 29 and 18. With r/R_o = 0.20 (and h/R_o = 0), a 40% increase is realized in Figure 18 by changing R/R_o from 1.5 to 2.0. With r/R_o = 0.20 and R/R_o = 1.5, a 160% increase is shown in Figure 29 by changing h/R_o from 0 to 0.20. Although this part of our study is far from conclusive, the available results indicate remarkable benefit of thin shields.

IV. SUMMARY AND CONCLUSIONS

This report presents the results of our exploratory numerical experiments on shock sensitivity of munitions. We have used the reactive hydrodynamic code 2DE to evaluate the posed problem[12] which covers three modes of detonation transfer, with twenty computations all listed in Tables I - III. The qualification of 2DE as a tool for numerical simulation was discussed at the outset. Our twenty computations describe the munition problem in detail which is not readily accessible by other approaches. Two distinct reactive flows are involved in the analogue, with shock waves communicable between them. The numerical aspects of these can serve to explain the mechanism and development of the detonation phenomena.

Shock waves play an essential role in all phases of the flow and reaction. Inert shocks are propagated in the gaseous products, steel casings, ambient air, and plastic shield - with patterns complicated by various interfaces or boundaries. Thus, cylindrical shocks behave distinguishably within the donor; their converging and diverging in the gases resemble a second explosion; and their reverberation in the casing spreads fluence forward and backward. Upon closing the air gap (if any), casing impact add multiple shocks to the scene. One after the other, shock pulses arrive at the acceptor explosive; it is the impact shock pulse, with a peak exceeding the LSGT 50% point, that evolves reactively into CJ-detonation, for the configurations investigated.

Our numerical results further offer a parameter analysis for shock initiation and loading, with

$$\eta_i = f_i\ (R/R_o,\ r/R_o,\ h/R_o, \xi\ )$$

depicted in Figures 18 - 29. A general trend of Figures 18 - 25 indicates that shock-sensitivity parameters η_i (i = 1,2···) tend to decrease as R/R_o or r/R_o increases. Such a trend may be used for practical purposes to scale or

---

[12] *Howe, P. M., Huang, Y. K., and Arbuckle, A. L., "A Numerical Study of Detonation Propagation between Munitions," The Seventh Symposium (International) on Detonation, Vol I (Preprint), pp 512-517 (June 1981).*

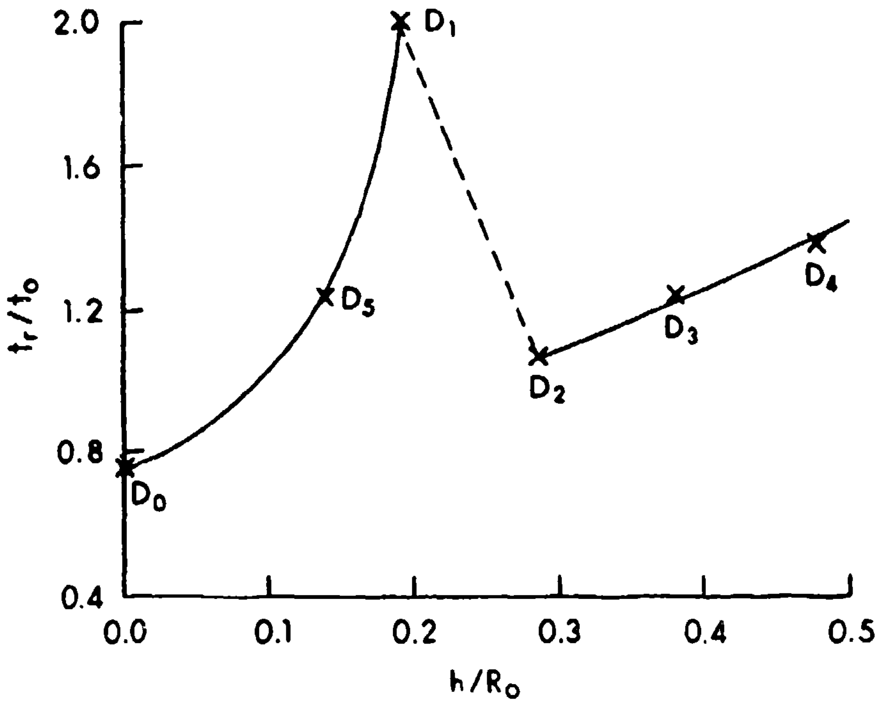

Figure 29 - N-Shape Curve Showing Variation of Time to Reaction with Shield Thickness

to interpolate detonation phenomena within the range of our numerical simulation, Figures 26 and 27 highlight the hypothesis that the impact shock pulse is essential for shock initiation. Yet it calls for special attention to check Figure 26 with Figure 22. At the first sight they seem to contradict each other. However, P_i and $\hat{P}$ refer to shock stimuli in two different phases of the initiation process, and one is bound to top the other. It is understandable that an out-of-phase trend prevails during shock buildup. The P^2t criterion is shown in Figure 28 to indicate the least chance for initiation to occur at $R/R_o = 1.5$, but it fails to confirm our result as validated with Figures 18 - 27. The trend of Figure 29 shows the remarkable benefits of thin plastic shields. It should be remarked that shock initiation can be affected by many factors - chemical, hydrodynamic, and structural. Our analysis has placed more emphasis on structural parameters, and further extension will have to be made.

For lack of comparable data, the accuracy of our numerical results may be questioned; but there should be no doubt about the state of art for our modeling[7]. It is anticipated that such situation will be improved in our subsequent work.

ACKNOWLEDGEMENTS

The authors wish to thank Dr. P. M. Howe for his able supervision, stimulating discussion, and many excellent suggestions throughout this investigation. Special thanks are due to Dr. J. Starkenberg who has read and helped strengthen the manuscript graciously. Finally, it would be impossible to present this report to the serious reader without the diligent and accurate typing of Mrs. D. L. Cianelli during this busy season of her clerical work.

DISTRIBUTION LIST

No. of Copies	Organization
12	Commander Defense Technical Info Center ATTN: DDC-DDA Cameron Station Alexandria, VA 22314
2	Commander US Army Materiel Development and Readiness Command ATTN: DRCDMD-ST DRCDE-DW 5001 Eisenhower Avenue Alexandria, VA 22333
4	Commander US Army Armament Research and Development Command ATTN: DRDAR-TSS (2 cy) DRDAR-LCE, Dr. R.F.Walker DRDAR-LCE, Dr. N. Slagg Dover, NJ 07801
1	Commander US Army Armament Materiel Readiness Command ATTN: DRSAR-LEP-L, Tech Lib Rock Island, IL 62199
1	Director US Army ARRADCOM Benet Weapons Laboratory ATTN: DRDAR-LCB-TL Watervliet, NY 12189
1	Commander US Army Aviation Research and Development Command ATTN: DRDAV-E 4300 Goodfellow Boulevard St. Louis, MO 63120
1	Director US Army Air Mobility Research and Development Laboratory Ames Research Center Moffett Field, CA 94035
1	Commander US Army Communications Rsch and Development Command ATTN: DRDCO-PPA-SA Fort Monmouth, NJ 07703
1	Commander US Army Electronics Research and Development Command Technical Support Activity ATTN: DELSD-L Fort Monmouth, NJ 07703
1	Commander US Army Missile Command ATTN: DRSMI-R Redstone Arsenal, AL 35809
1	Commander US Army Missile Command ATTN: DRSMI-YDL Redstone Arsenal, AL 35809
1	Commander US Army Missile Command ATTN: DRSME-RK, Dr. R.G. Rhoades Redstone Arsenal, AL 35809
1	Commander US Army Tank Automotive Rsch and Development Command ATTN: DRDTA-UL Warren, MI 48090
1	Director US Army TRADOC Systems Analysis Activity ATTN: ATAA-SL, Tech Lib White Sands Missile Range NM 88002
1	Commander US Army Research Office ATTN: Chemistry Division P.O. Box 12211 Research Triangle Park, NC 27709

DISTRIBUTION LIST

No. of Copies	Organization
1	Commander Office of Naval Research ATTN: Dr. J. Enig, Code 200B Arlington, VA 22217
1	Commander Naval Sea Systems Command ATTN: Mr. R. Beauregard, SEA 64E Washington, DC 20362
1	Commander Naval Explosive Ordnance Disposal Facility ATTN: Technical Library Code 604 Indian Head, MD 20640
1	Commander Naval Research Lab ATTN: Code 6100 Washington, DC 20375
1	Commander Naval Surface Weapons Center ATTN: Code G13 Dahlgren, VA 22448
8	Commander Naval Surface Weapons Center ATTN: Mr. L. Roslund, R122 Mr. M. Stosz, R121 Code X211, Lib E. Zimet, R13 R.R. Bernecker, R13 J.W. Forbes, R13 S.J. Jacobs, R10 K. Kim, R13 Silver Spring, MD 20910
4	Commander Naval Weapons Center ATTN: Dr. L. Smith, Code 3205 Dr. A. Amster, Code 385 Dr. R. Reed, Jr., Code 388 Dr. K. J. Graham, Code 3835 China Lake, CA 93555

No. of Copies	Organization
1	Commander Fleet Marine Force, Atlantic ATTN: G-4 (NSAP) Norfolk, VA 23511
1	Commander Edwards AFB ATTN: Mr. R. Geisler, Code AFRPL MKPA Edwards AFB, CA 93523
1	Commander Ballistic Missile Defense Advanced Technology Center ATTN: Dr. David C. Sayles P.O. Box 1500 Huntsville, AL 35808
1	Director Lawrence Livermore National Lab University of California ATTN: Dr. M. Finger Livermore, CA 94550
1	Director Los Alamos National Lab ATTN: Dr. B. Craig, M Division P.O. Box 1663 Los Alamos, NM 87545
1	Schlumberger Well Services ATTN: Dr. C. Aseltine 5000 Gulf Freeway Houston, TX 77023

Aberdeen Proving Ground

Dir, USAMSAA
ATTN: DRXSY-D
DRXY-MP, H. Cohen

Cdr, USATECOM
ATTN: DRSTE-TO-F

Dir, USACSL, Bldg 3516, EA
ATTN: DRDAR-CLB-PA

USER EVALUATION OF REPORT

Please take a few minutes to answer the questions below; tear out this sheet, fold as indicated, staple or tape closed, and place in the mail. Your comments will provide us with information for improving future reports.

1. BRL Report Number ______________________

2. Does this report satisfy a need? (Comment on purpose, related project, or other area of interest for which report will be used.)

____

____

____

3. How, specifically, is the report being used? (Information source, design data or procedure, management procedure, source of ideas, etc.) ______________________

____

____

4. Has the information in this report led to any quantitative savings as far as man-hours/contract dollars saved, operating costs avoided, efficiencies achieved, etc.? If so, please elaborate.

____

____

5. General Comments (Indicate what you think should be changed to make this report and future reports of this type more responsive to your needs, more usable, improve readability, etc.) ______________________

____

____

____

6. If you would like to be contacted by the personnel who prepared this report to raise specific questions or discuss the topic, please fill in the following information.

Name: ______________________

Telephone Number: ______________________

Organization Address: ______________________

____

____

FOLD HERE

Director
US Army Ballistic Research Laboratory
Aberdeen Proving Ground, MD 21005

NO POSTAGE NECESSARY IF MAILED IN THE UNITED STATES

OFFICIAL BUSINESS
PENALTY FOR PRIVATE USE, $300

BUSINESS REPLY MAIL
FIRST CLASS PERMIT NO 12062 WASHINGTON, DC

POSTAGE WILL BE PAID BY DEPARTMENT OF THE ARMY

Director
US Army Ballistic Research Laboratory
ATTN: DRDAR-TSB
Aberdeen Proving Ground, MD 21005

FOLD HERE